JQS Journal of Quaternary Science

Glacial landforms and their implications for glacier dynamics in Rijpfjorden and Duvefjorden, northern Nordaustlandet, Svalbard

O. FRANSNER,[1]* R. NOORMETS,[1] A. E. FLINK,[1] K. A. HOGAN,[2] M. O'REGAN[3] and M. JAKOBSSON[3]

[1]Department of Arctic Geology, University Centre in Svalbard, Longyearbyen 9171, Norway
[2]British Antarctic Survey, Cambridge CB3 0ET, UK
[3]Department of Geological Sciences, Stockholm University, Stockholm 10691, Sweden

ABSTRACT: Observations of subglacial landforms yielding the configuration and dynamics of former ice-flows have for the first time been made in Rijpfjorden and Duvefjorden, Nordaustlandet, Svalbard, using sub-bottom acoustic, swath-bathymetric data and sediment cores. Five acoustic-stratigraphic units were distinguished suggesting the presence of a complete glacial–postglacial succession in the central fjord basins. ^{14}C ages from the sediments indicate that the inner Rijpfjorden and central Duvefjorden were deglaciated before ca. 10.6 cal ka BP and 11.0 cal ka BP, respectively. Maximum sediment thickness in Rijpfjorden and Duvefjorden is 26 m, resulting in sediment accumulation rates of ca. 66 cm ka^{-1}. The landform record suggests that the ice streaming in both fjords was topographically controlled. The considerably deeper basin and higher elongation ratios of the crag-and-tails in Duvefjorden are linked to the faulted bedrock and possibly to somewhat larger ice stream and/or more focused ice-flow compared to that in Rijpfjorden. De Geer moraines suggest slower retreat of a grounded ice margin from shallow areas of Rijpfjorden. In deeper areas of the fjords, the glaciers were probably floating, resulting in the lack of ice-marginal transverse landforms. The ice margin retreat from these areas was probably relatively rapid and dominated by calving. Copyright © 2017 John Wiley & Sons, Ltd.

KEYWORDS: Late Weichselian; glacial landforms; deglaciation; ^{14}C ages; Nordaustlandet.

Introduction

Ice sheets are important for the global climate system (e.g. NAD Science Committee, 1992). Particularly important are the marine-based ice sheets that are resting below sea level as they are most exposed and vulnerable to the sea level rise associated with climate warming (Patton et al., 2015; Stokes et al., 2015). Most of the mass-loss from the marine-based ice sheets occurs through calving at the margins of marine-terminating ice streams that rapidly transport ice from the interior of the ice sheet to its margins (Rignot and Kanagaratnam, 2006). Ice streams are therefore important for relatively fast changes in ice sheet mass-balance and associated oceanographic changes at high latitudes (Bond and Lotti, 1995).

The Svalbard-Barents Sea Ice Sheet (SBIS) was marine-based during the Late Weichselian and was drained through numerous ice streams flowing in the cross-shelf troughs of the Barents Sea during the Last Glacial Maximum (LGM) (Siegert et al., 2001; Andreassen et al., 2004; Ottesen et al., 2005; Robinson and Dowdeswell, 2011). These ice streams were often sourced in the major fjord valleys where the underlying topography resulted in the confluence of glaciers. On the western Svalbard shelf, all cross-shelf troughs are linked to major fjord systems (Ottesen et al., 2005).

The drainage patterns and deglaciation history in cross-shelf troughs along the western margin of the former SBIS are relatively well established due to numerous expeditions there (e.g. Andreassen et al., 2004, 2008; Landvik et al., 2005; Ottesen et al., 2005, 2007; Winsborrow et al., 2010; Rüther et al., 2011; Bjarnadóttir et al., 2013; Rebesco et al., 2014). Off eastern and northern Svalbard, the drainage patterns and deglaciation history are known only in general terms (e.g.

Ottesen et al., 2007; Dowdeswell et al., 2010; Hogan et al., 2010a,b). This is mainly due to the remoteness of these areas from the nearest ports and generally harsh sea ice conditions. However, decreasing sea ice extent has given easier access to surface vessels, which has resulted in several studies over the recent years from these areas (e.g. Hogan et al., 2010a,b; Batchelor et al., 2011; Chauhan et al., 2014, 2016a,b).

It has been established that the ice sheet reached the shelf edge north of Svalbard during the LGM (Knies et al., 2001; Chauhan et al., 2016a) and that fast-flowing ice reached there mainly through Hinlopen, Albertini and Kvitøya Troughs (Hogan et al., 2010b; Batchelor et al., 2011; Noormets et al., 2012). Retreat of the ice sheet from the shelf edge in this area begun ca. 18.5 ka (Knies et al., 2001; Chauhan et al., 2016a).

The aim of this paper is to improve our understanding of and further constrain the configuration and dynamics of the marine-based BSIS along its relatively poorly known northern Barents Sea margin. This includes better constraining the character and timing of deglaciation of the inner shelf and the fjords of Rijpfjorden and Duvefjorden in northern Nordaustlandet, using new high-resolution swath-bathymetric and sub-bottom acoustic data together with sediment core analyses.

Geological and glaciological setting

The Svalbard Archipelago is located at the north-western margin of the Barents Sea (Fig. 1a). The Barents Sea shelf and the Svalbard Archipelago formed because of tectonic uplift after the Eocene rifting, break up and opening of the Norwegian–Greenland Sea (Faleide et al., 1996). After the uplift, the region was shaped by the Plio-Pleistocene glacial–interglacial processes (Mangerud et al., 1998; Knies et al., 1998). Major morphological imprints of the glacial cycles on the Barents Sea shelf and the Svalbard Archipelago are the

*Correspondence to: O. Fransner, as above.
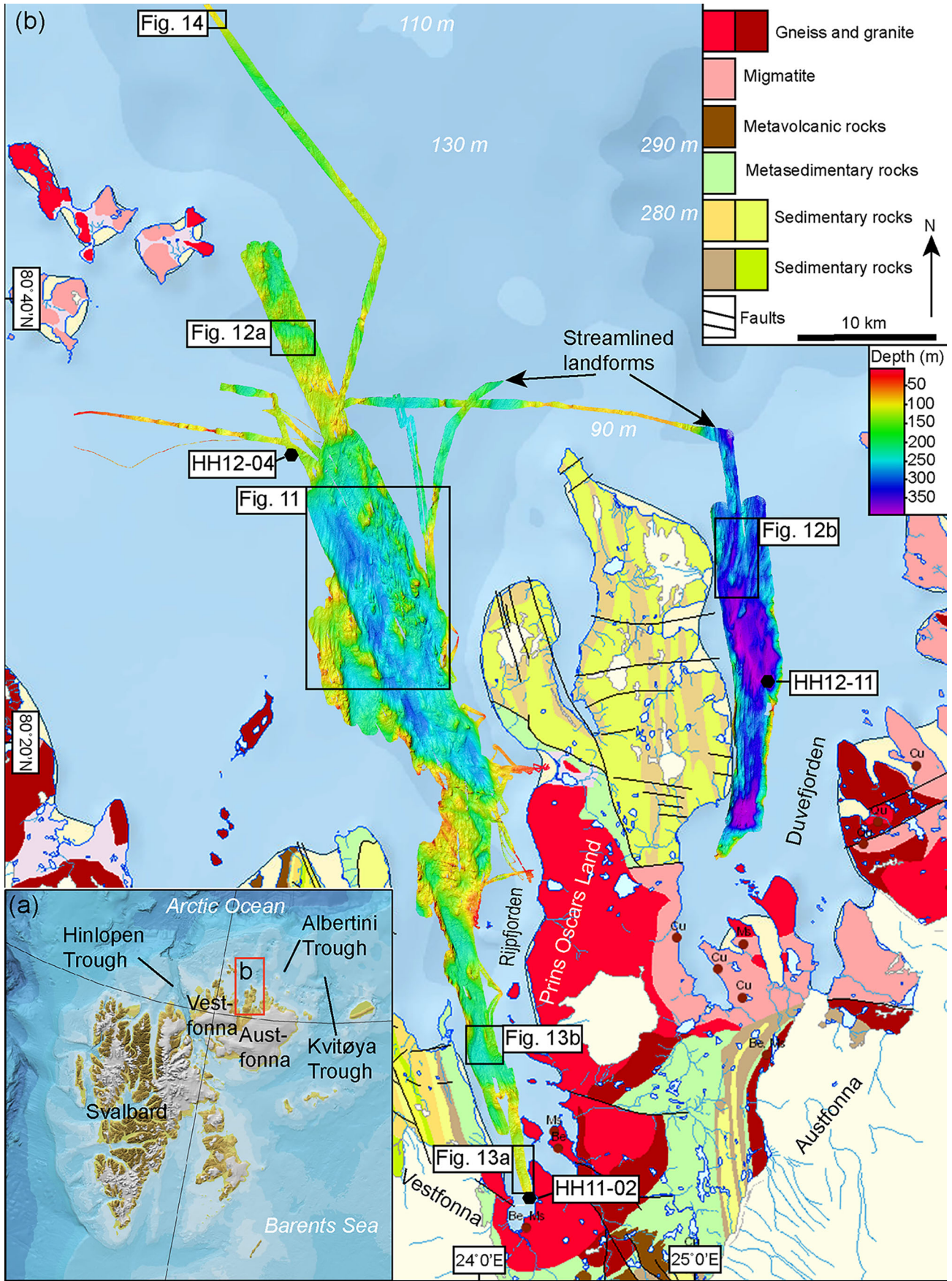E-mail: oscarjacob.fransner@unis.no

Figure 1. (a) IBCAO map showing the location of the study area and place names mentioned in the text. (b) Swath-bathymetric coverage of the study area. The three gravity core locations (HH11-02, HH12-04 and HH12-11) are marked with black hexagons. Streamlined landforms north of Rijpfjorden and Duvefjorden are arrowed. The study area is relatively faulted, especially Prins Oscars Land, where both E–W- and NW–NE-trending faults are present. The geological map of ice-free land areas is modified from online Svalbardkartet by Norsk Polarinstitutt. Background bathymetry data are from IBCAO version 3.0 (Jakobsson et al., 2012).

cross-shelf troughs and fjords eroded by streaming glacier ice draining the ice sheet (Ottesen *et al.*, 2007; Batchelor and Dowdeswell, 2014). Hinlopen and Kvitøya Troughs are two major cross-shelf troughs on the northern Svalbard margin that were occupied by streaming ice during the LGM (Koc, *et al.*, 2002; Hogan *et al.*, 2010b; Batchelor *et al.*, 2011). These troughs have a S–N orientation and reach the continental shelf edge (Hogan *et al.*, 2010b; Batchelor *et al.*, 2011).

Nordaustlandet is the second largest island of the Svalbard Archipelago situated in its north-eastern part between the Hinlopen and Kvitøya Troughs to the east and west of it, respectively (Fig. 1a). Rijpfjorden and Duvefjorden are two major fjords shaping the landscape of the northern Nordaustlandet, west and east of Prins Oscars Land, respectively (Fig. 1b). Both fjords have a S–N orientation and are open to the Arctic Ocean in the north (Fig. 1b). According to the coarse bathymetry map IBCAO, the respective maximum water depth north of Rijpfjorden and Duvefjorden is 130 and 290 m, respectively (Fig. 1b).

The geology of the ice-free parts of northern Nordaustlandet is dominated by Caledonian Rijpfjorden granite and migmatite (Flood *et al.*, 1969; Dallmann *et al.*, 2002; Johansson *et al.*, 2005). Sedimentary and metasedimentary rock types are present as well (Fig. 1b). Bedrock off the northern Nordaustlandet is dominated by the Hecla Hoek formation of Late Precambrian crystalline rocks (Elverhøi and Lauritzen, 1984). Unconsolidated sediments deposited during and after the last glacial are often found on top of the bedrock in the northern Barents Sea region and comprise three lithofacies (from bottom to top): (i) diamicton, (ii) pebbly mud and (iii) massive Holocene mud (Elverhøi *et al.*, 1989). Sediments older than the last glacial are preserved on the continental slope (Knies *et al.*, 2001; Chauhan *et al.*, 2016a, b). These sediments are influenced by mass-flow processes, contour currents as well as sediment deposition from sea ice and icebergs (Chauhan *et al.*, 2016b). During the LGM, the ice sheet margin reached the continental shelf edge north of Nordaustlandet ca. 23–22 cal ka BP and its retreat from the shelf edge started ca. 18.5 cal ka BP (Chauhan *et al.*, 2016a). The two ice caps, Vestfonna and Austfonna, are presently covering most of Nordaustlandet (Hagen *et al.*, 1993).

Data acquisition and methods

The data used here were acquired during UNIS cruises on R/V *Helmer Hanssen* during 2011 and 2012. The multibeam bathymetric and acoustic sub-bottom data were acquired using a hull-mounted Kongsberg EM300, 30-kHz multibeam

echo sounder system and Edge Tech 3300 chirp sub-bottom profiler.

The multibeam bathymetric data were gridded with 5–10-m isometric grid cell size and visualized using QPS Fledermaus software. The gridded data were exported to Arc Map (version 10.1) where the maps of glacial landforms were produced.

The sub-bottom data were processed and analysed in Kingdom Suite (version 8.8). A sound velocity of $1500 \, \mathrm{m \, s^{-1}}$ was used for converting the two-way travel-time (TWT) to depth which has been used earlier (e.g. Hogan *et al.*, 2011; Hjelstuen *et al.*, 2013). The digitized acoustic horizons were gridded in the Kingdom suite. The acoustic facies distinguished on the chirp data were correlated with sedimentological data based on three gravity cores which were analysed in the Department of Geological Sciences at Stockholm University, Sweden. A GeoTek multi-sensor core logger was used to measure P-wave velocity, bulk density and magnetic susceptibility in 1-cm intervals. The quality of the density measurements is dependent on the amplitude of the P-wave velocity. Therefore, densities related to P-wave velocities with amplitudes lower than 70% were removed. Clear spikes in magnetic susceptibility were also removed. The cores were also analysed in the ITRAX core scanner for acquiring radiographic images. The radiographic images were acquired with a resolution of 0.2 mm. Shear strength was measured in 5-cm intervals using a Controls group liquid limit penetrometer. A Malvern Master Sizer 3000 laser particle size analyser was used to measure the grain size distribution of the fine fraction (<1 mm) for sediment samples taken in 10-cm intervals. In sections with rapid variations (e.g. thin layers) samples were taken in up to 1-cm intervals. Sixty-five samples were wet-sieved for extracting the organic matter for ^{14}C dating. Tests of foraminifera, shells and shell fragments were picked from the > 125-μm fraction, and from the > 63-μm fraction in samples where the organic material was scarce. Seven samples were dated using single stage accelerator mass spectrometry (SSAMS) in the radiocarbon dating laboratory at Lund University, Sweden. Two ages were based on mixed benthic foraminifera, three on shell fragments and two on a *Buccium glaciale* and a paired *Thyasira flexulosa*, respectively (Table 1).

The ^{14}C ages were calibrated to calendar years using Calib 7.1 with the Marine13 calibration curve, which has a default marine reservoir correction of 405 years (Reimer *et al.*, 2013). This marine reservoir correction was applied for direct comparison with Chauhan *et al.* (2016a). The calibrated ages are shown in 1sigma and 2sigma (Table 1). The sedimentation

Table 1. SSAMS 14C dates and sedimentation rates for cores HH11-02 and HH12-11. The sedimentation rates are based on mean 1sigma ages.

HH11-02 Inner Rijpfjorden

Depth (cm)	Material used	^{14}C age	Cal. age BP 1 sigma	Cal. age BP 2sigma	Sed. rate (cm/ka)
184-185	*Buccinum glaciate*	8695-8785	9376-9470	9299-9499	20
225-226	Shell fragments	9645-9745	10531-10658	10464-10738	35

HH12-11 Central Duvefjorden

| Depth (cm)	Material used	^{14}C age	Cal. age BP 1sigma	Cal. age BP 2sigma	Sed. rate (cm/ka)
11-12	Paired bivalve (*Thyasira flexulosa*)	755-895	393-518	297-551	26
47-48	Shell fragments	1665-1775	1224-1298	1174-1336	45
220-221	Shell fragment	5900-5980	6300-6390	6270-6441	34
359-363	Mixed benthic foraminiferas	8865-8965	9503-9621	9463-9704	44
447-453	Mixed benthic foraminiferas	9890-10000	10813-11023	10727-11095	66
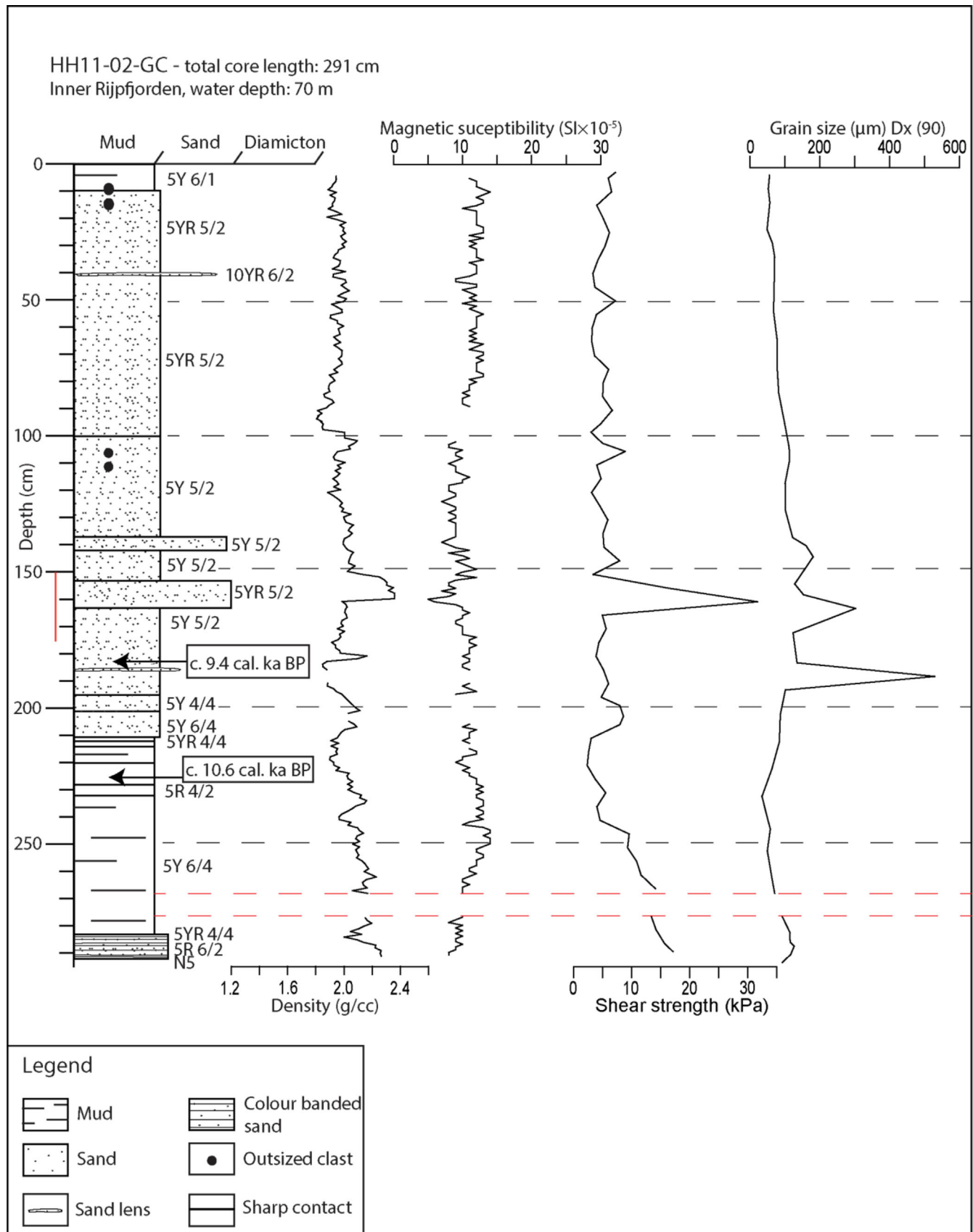
Figure 2. Lithological log with Munsell colour codes and calibrated ^{14}C ages of the gravity core HH11-02 from the inner Rijpfjorden. The graphs show physical properties (density, magnetic susceptibility, shear strength and grain size) of the core. Note that the sand layer at 41 cm core depth was considered too coarse to be analysed in the Malvern mastersizer 3000. The dashed red lines show areas of major physical disturbance which gives unreliable results of the physical properties. The red line along the scale bar at 150–175-cm indicates the location of Fig. 3a. The lithological units are described in detail in the text. The location of the core is shown in Fig. 1b.

rates were calculated by linear interpolation between the mean 1sigma values of each sample. The respective mean 1sigma values are used throughout the text where ages are mentioned.

Sedimentological data

HH11-02

Description

The 291–cm-long HH11-02 core was acquired from the inner Rijpfjorden (Fig. 1b). From the core, two samples were radiocarbon dated (Table 1). The upper 10 cm of the core consists of light olive grey (5Y 6/1 in Munsell colour chart) massive mud with a small amount of outsized clasts (Fig. 2). This section is followed by a pale brown to pale yellowish brown (5YR 5/2 to 10YR 6/2) 200-cm-thick, relatively mica-rich silty sand layer with four coarse sand layers embedded in it. The top coarse sand layer is found at 41.5–42.5 cm and has the colour 10YR 6/2. This layer has sharp transitions to the surrounding silty sand (Fig. 2). The following sand layers are found at 137–142, 153–163 and 186–186.5 cm, respectively. The four sand layers are characterized by sharp contacts and a relatively high grade of compaction. The thickest coarse sand layer is pale brown (5YR 5/2) and contains a brighter coloured (5R 6/2) deformed layer which is < 1 cm thick. The deformed layer has the same grade of compaction and grain size as the surrounding sand (Fig. 2). A radiographic image illustrates the embedded coarse sand layer at 153–163 cm and its sharp transitions to the silty sand (Fig. 3a). At 184–185 cm core depth, the silty sand is dated to ca. 10.6 cal ka BP using an intact gastropod (*Buccinum glaciale*) (Table 1).

The silty sand is followed by a light olive grey (5Y 6/4) mud that contains diffuse, 1–6-cm-thick reddish bands (5YR 4/4 to 5R 4/2). The mica concentration in the mud is somewhat lower compared to in the silty sand. The grain size of the mud is slightly finer than the mud lithofacies in the top layer of the core. At 225–226 cm core depth, the mud is dated to ca. 9.4 cal a BP using shell fragments (Table 1). At 281–291 cm core depth, the lithology consists of a fine-grained sand unit with colour bands (0.5 cm thick) where brown, pale red and light grey (5YR 4/4, 5R 6/2, N5) units alternate. Foraminifera and shell fragments are rare throughout the core.

The density of the sediment in HH11-02 core is 1.8–2.4 g ml^{-1}. The highest values are characteristic to the coarse sand units in the middle of the core, whereas the lowest values are found in the upper 95 cm of the core (Fig. 2). The magnetic susceptibility shows relatively little variation in its values, which are 5–15 SI × 10^{-5}Author: please confirm the units for magnetic susceptibility. The lowest values are found in the coarse-grained layers of the core (Fig. 2). The shear strength shows values from 2.5 to 32 kPa (Fig. 2). However, the maximum value of 32 kPa is not representative as the fall cone method is not adequate for sand. The lowermost 25 cm of the core shows a gradual increase in shear strength from 10 to 17 kPa (Fig. 2). The Dx(90) grain sizes vary from 34 to 560 μm with the highest values recorded in the two sand layers in the middle of the core and a sand lens at 187 cm (Fig. 2). Density, shear strength and grain size are positively correlated, which is particularly clear in the coarser-grained layers, whereas magnetic susceptibility shows an inverse correlation to these parameters (Fig. 2).
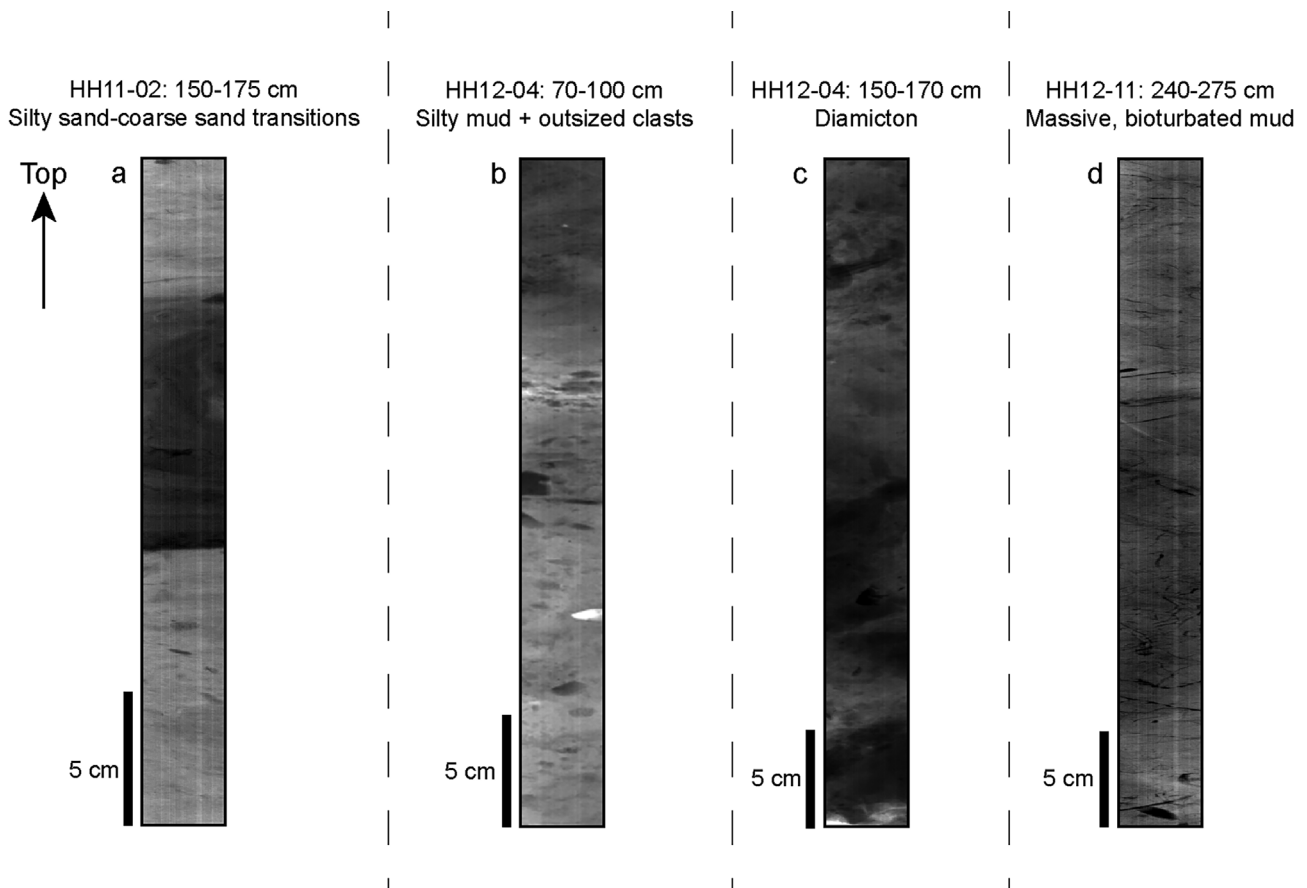

Figure 3. Radiographic images of the major lithofacies from cores HH11-02, HH12-04 and HH12-11. (a) Sharp transitions from silty sand to coarse sand and back to silty sand. (b) Mud rich in outsized clasts. (c) Diamicton with mud lenses. (d) Massive, bioturbated mud.

Interpretation

The massive mud at 0–10 and 210–281 cm is interpreted as marine mud. This is based on its homogeneous fine-grained composition indicating a low-energy depositional environment through suspension settling (Elverhøi and Solheim, 1983). This sediment type is common in the northern Barents Sea (Elverhøi and Solheim, 1983). Rare outsized clasts further indicate little ice-rafted debris (IRD) production (Plassen et al., 2004). The similar colour and composition of the massive mud in the top and bottom of the core further indicate a similar source for these sediments.

The silty sand (10–210 cm) indicates a depositional environment highly influenced by increased meltwater input. This is based on the coarser grain size of the silty sand as well as on its higher mica concentration, which normally indicate changed lithology of the sediment source (Plassen et al., 2004). IRD can be excluded due to the lack of outsized clasts (Elverhøi and Solheim, 1983). The four coarse sand layers embedded in the silty sand are interpreted as mass-flow events. This is based on

their coarser and more angular grains and sharp contacts to the above and underlying mud layers, implying a short transportation and fast deposition of these layers. Changed lithology is also supported by the significant difference in magnetic susceptibility of the coarse sand layer at 153–163 cm. Similar mass flows as envisaged here have been described in the fjords of Svalbard (Ottesen and Dowdeswell, 2006), and resulting sand layers with correlated changes in magnetic susceptibility are, for example, found in Fensfjorden and Austfjorden, Norway (Hjelstuen et al., 2013). The fine-grained sand layer without outsized clasts at 281–291 cm suggests a similar depositional environment as for the silty sand. However, the sharp colour variations are interpreted as variations in lithology of the sediment source (Plassen et al., 2004).

HH12-04

Description

The 173-cm-long HH12-04 core was acquired on the inner shelf off Rijpfjorden (Fig. 1b). Three lithofacies were
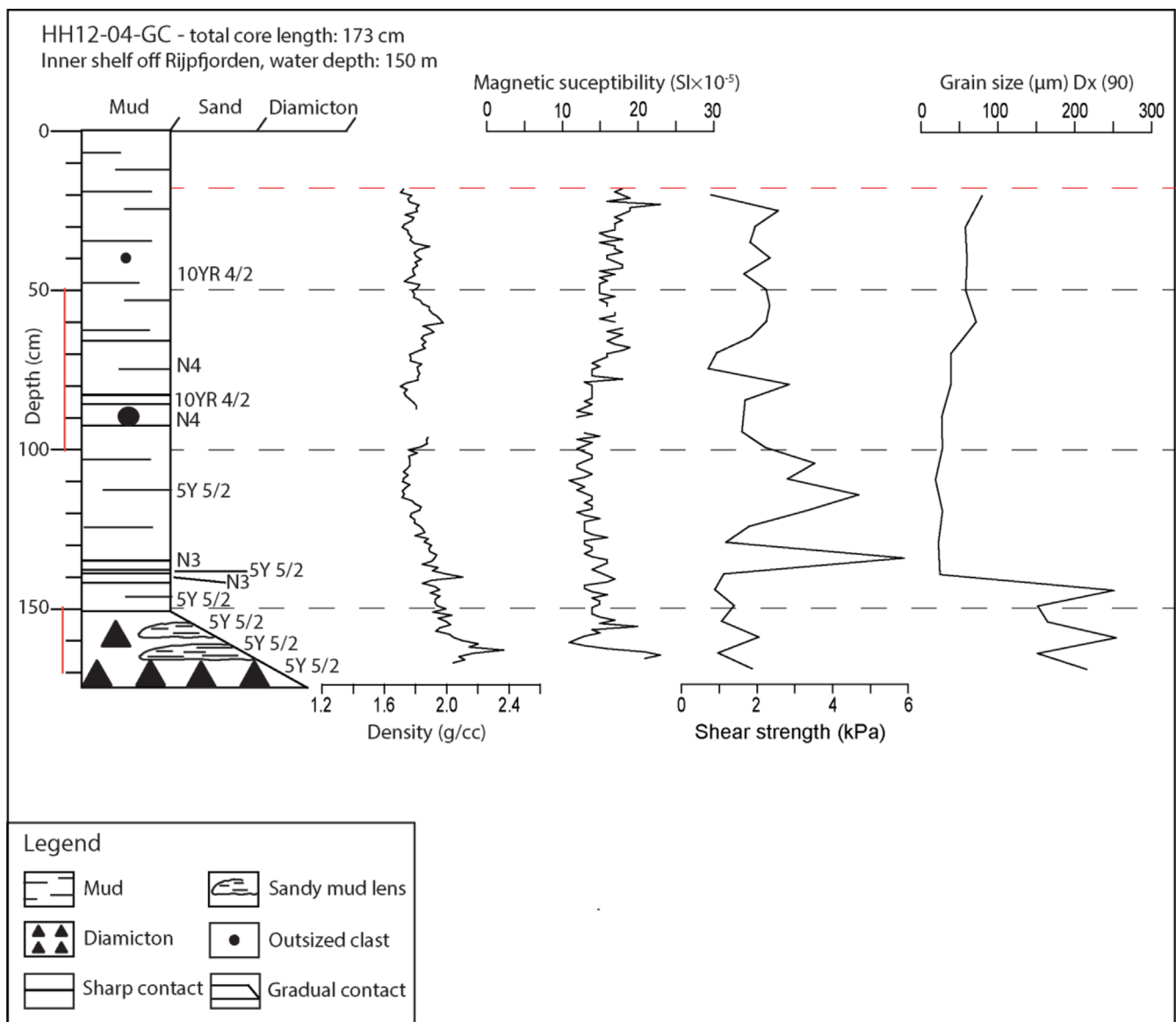

Figure 4. Lithological log with Munsell colour codes and physical properties (density, magnetic susceptibility, shear strength and grain size) of the gravity core HH12-04 from the inner shelf north of Rijpfjorden. The core is dominated by two lithofacies of mud (massive and outsized clast-rich) and a fining-upwards diamicton facies at the base. The values of the physical properties corresponding to the first 19 cm of the core were considered unreliable due to physical disturbance of the sediments indicated by the dashed red line at 19 cm. The physical properties above this line have been omitted. The red lines along the scale bar at 70–100 and 150–170 cm indicate the location of Fig. 3b and c, respectively. The lithological units are described in detail in the text. The location of the core is shown in Fig. 1b.
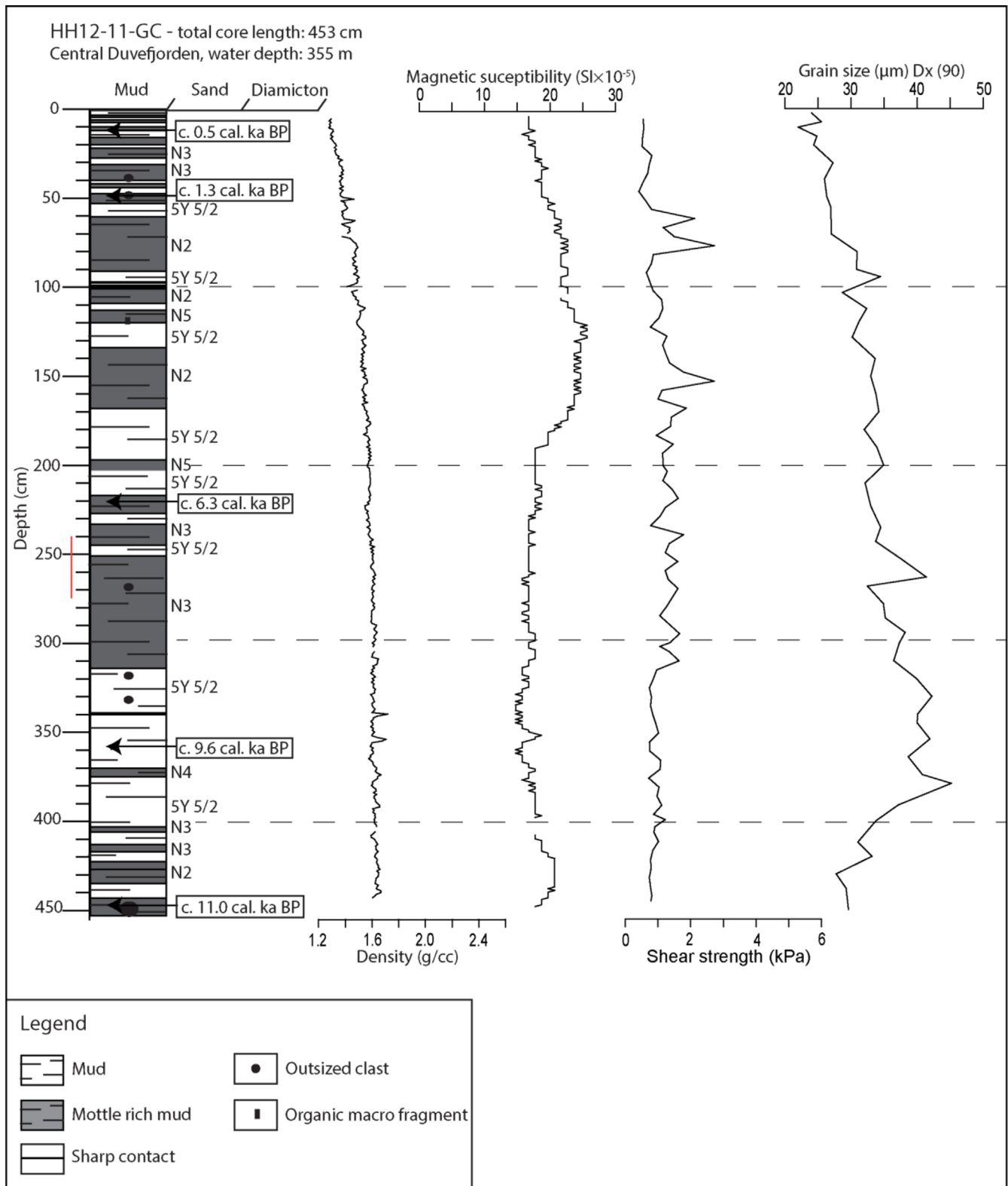
Figure 5. Lithological log with Munsell color codes, calibrated ^{14}C ages and physical properties (density, magnetic susceptibility, shear strength and grain size) of the gravity core HH12-11 acquired from the central Duvefjorden. The red line along the scale bar at 240–275-cm indicates the location of Fig. 3d. The lithological units are described in detail in the text. The location of the core is shown in Fig. 1b.

distinguished: (i) massive silty mud, (ii) silty mud rich in outsized clasts and (iii) diamicton (Fig. 4). Silty muds, both massive and with a relatively high ratio of outsized clasts (estimated to 10–20%), are the dominating lithofacies types in the HH12-04 core. The massive mud comprises 0–66 cm of the core, but changes to mud with a higher content of outsized clasts (<20 mm in diameter) between 66 and 149 cm (Fig. 4). The radiographic image of the core interval

70–100 cm reveals outsized clasts visible as relatively dark spots (Fig. 3b). The colour of the mud generally varies from dark yellowish brown to medium grey (10YR 4/2 to N4) with sharp transitions in between. Locally, olive grey (5Y 5/2) intervals are also present. The tickness of the differently coloured mud layers varies from 60 to 1–2 cm. Foraminifera are rare in the mud. From 151 to 173 cm, the core is dominated by coarse sand that changes gradually to
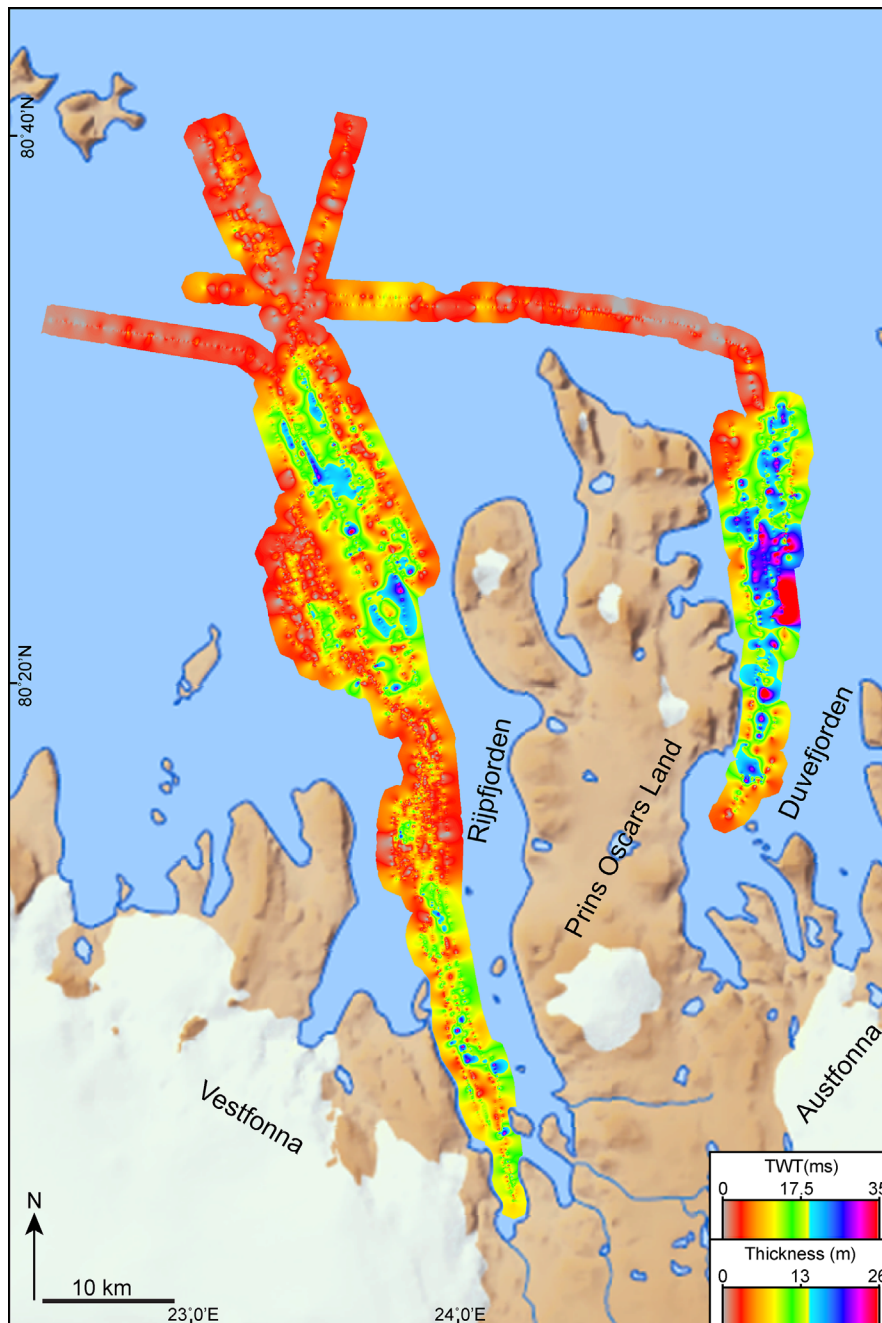
Figure 6. Total thickness of deglacial and postglacial sediments in Rijpfjorden and Duvefjorden and on the inner shelf north of the fjords. The thickness in metres is based on a sound velocity of $1500\,\mathrm{m\,s^{-1}}$.

diamicton with subangular clasts with up to 20-mm-long *a*-axes (Fig. 4). The diamicton contains two olive grey (5Y 5/2) sandy mud lenses. In the radiographic image, the diamicton appears darker than the mud lenses (Fig. 3c).

The density of the sediments in HH12-04 core varies from 1.7 to $2.4\,\mathrm{g\,ml^{-1}}$, higher values being typically at the lower part of the core, corresponding to the diamicton (Fig. 4). Magnetic susceptibility varies from 11 to 23 $\mathrm{SI}\times10^{-5}$ and shows a significant anomaly at 75 cm, where the magnetic susceptibility first drops and then gradually increases down-core. This gradual increase correlates with the top of the silty mud rich in outsized clasts. Shear strength varies from 0.7 to 6 kPa and shows highest variations at the depths correlated with the silty mud rich in outsized clasts. The Dx(90) grain size varies from 19 to 272 μm (Fig. 4). Grain size decreases downwards until 141-cm core depth. The highest grain size values are found in the diamicton. The variation of the grain size in the lower part of the core corresponds to the sandy mud lenses in the diamicton (Fig. 4). Magnetic susceptibility is negatively correlated with shear strength except for in the
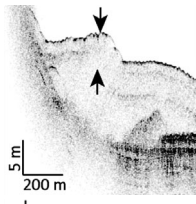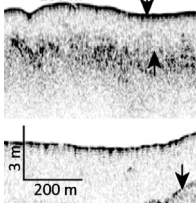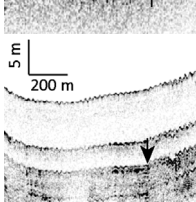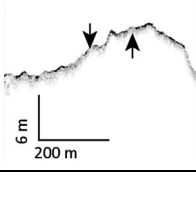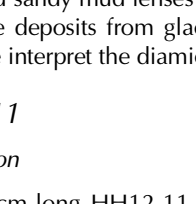
diamicton (Fig. 4). The top 19 cm is not presented on the physical properties logs due to physical disturbance in the core (Fig. 4).

Interpretation

The massive mud in the uppermost 66 cm of the core was probably deposited in a similar environment as the massive mud in HH11-02. This is based on the similar grain size and physical properties of these sediments (Fig. 2 and 4). The high concentration of outsized clasts in the relatively fine-grained mud between 66 and 149 cm indicates a glaciomarine depositional environment highly influenced by IRD. Similar pebbly mud from the central and northern Barents Sea is described by Elverhøi and Solheim (1983) and in Kvitøya Trough (Hogan et al., 2010b).

The low shear strength of the upwards-fining diamicton at the base of HH12-04 suggests the diamicton to be either subglacial deformation till (e.g. Alley et al., 1987; Hogan et al., 2010b), or dropstone diamicton (possibly basal meltout-till)

Table 2. Description and interpretation of the acoustic units identified from the chirp data from Rijpfjorden and Duvefjorden. Each unit is arrowed in the chirp example column.

Acoustic unit	Chirp example	Description	Interpretation
5		Acoustically transparent or chaotic lobes. The upper bounding reflector is of moderate to high amplitude and medium continuity. Unit 5 is present at the foot of steep slopes (Fig. 7d).	The acoustic characteristics of unit 5, its lobate geometry and particularly the location at the foot of steep slopes are common for mass-flow deposits (e.g. Hogan et al., 2011).
4		Acoustically transparent unit. Locally semi-transparent in the inner fjords. The upper bounding reflector is of high amplitude and high continuity. Normally unit 4 is the topmost unit but is covered by unit 5 when present (Fig. 7c).	Unit 4 was found in all three gravity cores (Figs 8-10). The 14C dates from HH11 -02 and HH12-11 cores infer a Holocene age of this unit. Interpreted as marine mud with a higher content of sand in the inner Rijpfjorden compared to the inner shelf and in the central Duvefjorden.
3		Acoustically transparent unit. Locally semi-transparent in the inner fjords. The amplitude of the upper bounding reflector is usually low and of moderate continuity.	The transparent reflection signature infers a homogenous composition. Interpreted as glacimarine, uniform mud that probably has a high sand content in inner Rijpfjorden based on the fine sand-rich mud recovered in the lowermost 10 cm of HH11-02 (Fig. 2).
2		The reflection geometry contains multiple reflectors of medium to high amplitude and moderate continuity. The reflectors are semi-parallel to parallel to each other and to the acoustic basement. Locally, disturbed areas with chaotic acoustic signature occur. The upper bounding reflector is of moderate to high amplitude and high continuity.	The parallel to semi-parallel conformal reflection geometry of unit 2 infers a semi-rhythmically varying sediment composition or structure. This is characteristic for glacimarine laminated mud formed due to seasonal variations in glacial melt-out deposits. Similar sediments have been reported in several Spitsbergen fjords (Plassen et al., 2004).
1		High amplitude and high continuity top reflector. Little to no penetration of acoustic signal below this reflector. This unit represents the acoustic basement and is either subcropping on the sea floor or is covered with a thin layer of unit 2 or 4 deposits.	Sampled by HH 12-04 and therefore identified as diamicton. However, different moraine types and bedrock cannot be distinguished based on their acoustic character alone. Therefore, U1 may consist of bedrock in other areas.

(e.g. Harland *et al.*, 1966; Dreimanis, 1979). Based on the embedded sandy mud lenses in diamicton, probably representing plume deposits from glacial meltwater discharge (Powell, 1984), we interpret the diamicton to be a basal meltout.

HH12-11

Description

The 453-cm-long HH12-11 core was acquired from a basin of 355 m water depth in the central Duvefjorden (Fig. 1b). Massive mud dominates throughout the core (Fig. 5). This mud displays a mottle-rich, medium dark grey to dark grey (N3–N2) and light olive grey (5Y 5/2) units (Fig. 5). Bioturbation is present throughout the core, particularly between 100 and 300 cm. Bioturbation is shown as black, thread-like microburrows on the radiographic images of the core (Fig. 3d). Microburrows are easily distinguished in radiographic images when they are pyritized (Löwemark *et al.*, 2006). Foraminifera are rare throughout the core. The most common species are *Nonionella labradorica*, *Elphidium excavatum* and *Epistominella exigua*. Outsized clasts are rare, but when present they are subangular with diameters of 1–5 mm. The base of the core contains one subrounded granitic clast with the dimensions of 65 × 50 × 25 mm.

The density of sediments in the HH12-11 core varies from 1.3 to 1.7 g ml^{-1}. The lowest values are found at the top, increasing gradually towards the bottom of the core (Fig. 5). Magnetic susceptibility varies between 15 and 26 SI × 10^{-5} and increases downwards in the core until 160 cm from where it is relatively constant until 350 cm followed by another increase to 440 cm (Fig. 5). Shear strength varies from 0.4 to 2.7 kPa and has the highest values between 50 and 310 cm of the core (Fig. 5). Grain size varies from 22 to 46 μm coarsening downwards until 380 cm core depth, from where it decreases until the base of the core (Fig. 5). Five radiocarbon dates were acquired from HH12-11 (Table 1). These dates reach from ca. 0.46 to 11 ca ka BP.

Interpretation

Based on the ^{14}C dates, the massive and often bioturbated mud present throughout HH12-11 is Holocene marine mud, deposited under similar conditions as the massive mud of HH11-02 and HH12-04. The mottles in the mud are monosulphides, which are relatively common in this type of mud (Elverhøi *et al.*, 1989). The outsized clasts in the core are interpreted as IRD, which is supported by their subrounded geometries and their scattered distribution, suggesting glacial erosion and transportation. IRD is common in the northern Barents Sea (Elverhøi and Solheim, 1983; Hogan *et al.*, 2010b). The wide range of rock types of northern Nordaustlandet makes provenance interpretations difficult (Fig. 1b).
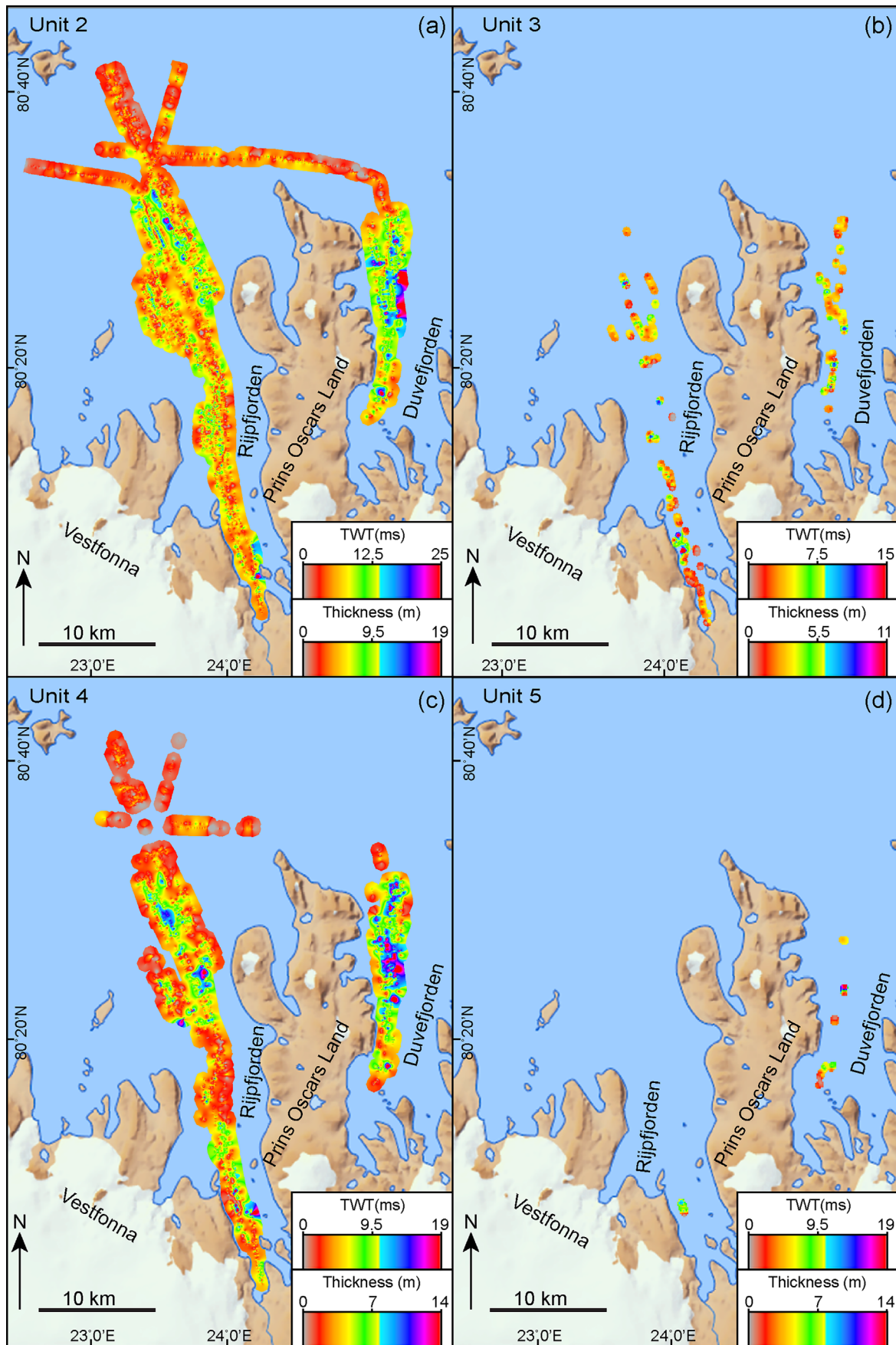
Figure 7. Thickness and distribution of acoustic units 2 (a), 3 (b), 4 (c) and 5 (d). The thickness scale bars in metres are based on sound velocity of 1500 m s^{-1}.
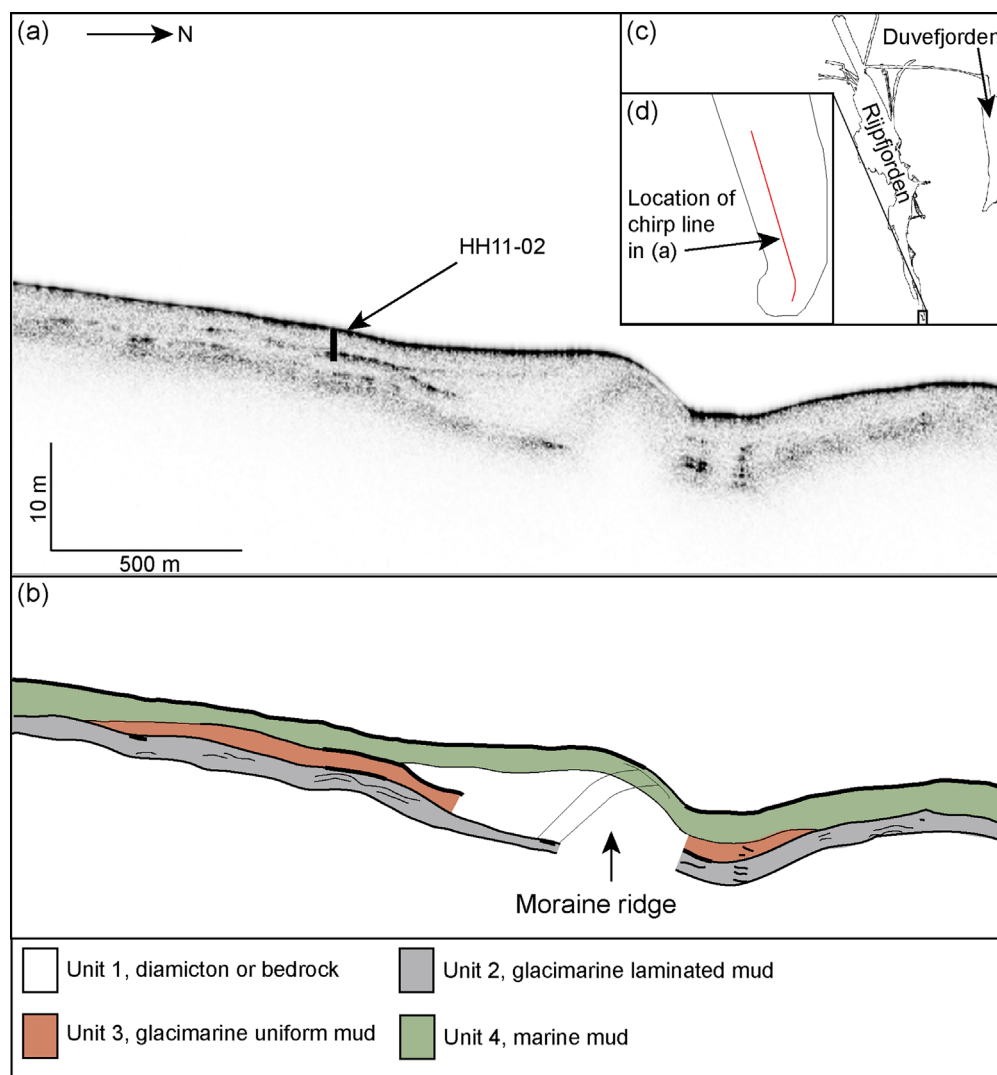
Figure 8. (a) Chirp profile showing the location and approximate penetration depth of core HH11-02 (arrowed). (b) Interpretation of the chirp profile in (a) based on the acoustic facies analysis and the lithology of HH11-02. (c,d) The location of the chirp profile, which is marked with a red line in (d).

However, the IRD in HH12-11 probably originated from the onshore bedrock surrounding Duvefjorden. The significant increase in sedimentation rate at ca. 1.3 cal ka BP and the higher values in magnetic susceptibility indicate increased sediment input of different lithology, probably due to increased meltwater input (Plassen *et al.*, 2004).

Chirp sub-bottom data

The total sediment thickness of deglacial and postglacial sediments in Rijpfjorden and Duvefjorden varies from 0 to 35 ms TWT (or 0–26 m based on a sound velocity of 1500 m s^{-1}) (Fig. 6). Thickest sediment successions are found in the deepest areas of the fjords, whereas the inner shelf and the relatively shallow areas of the fjords are characterized by relatively thin or absent sediment cover (Fig. 6). Based on acoustic characteristics, five units were distinguished in the acoustic stratigraphy (U1–U5, from base to top). The acoustic characteristics and interpretations of the units are presented in Table 2. Isopach maps are presented for each unit (Fig. 7).

Interpretation of the acoustic units and correlation with sediment cores

Inner Rijpfjorden – HH11-02

A buried ridge-shaped feature consisting of the acoustic unit U1 is present at the core location of HH11-02 (Fig. 8).

Although the acoustic characteristics of U1 alone are not sufficient to distinguish diamicton and bedrock, the ridge shape of the buried feature indicates a buried moraine similar to findings in Isfjorden (Plassen *et al.*, 2004). The conformal draping of U2 indicates an ice-proximal glaciomarine environment of inner Rijpfjorden during deposition (cf. Hogan *et al.*, 2011) (Fig. 8). The base of HH11-02 correlates with U3, indicating a glacimarine mud with relatively high sand content, indicating influence of meltwater input during deglaciation (cf. Plassen *et al.*, 2004) (Fig. 8). U4 is conformably overlying U3 (Fig. 8). The overall acoustic transparency of U4 and its fine grain size together with ^{14}C ages in HH11-02 indicate deposition through suspension settling during the Holocene (cf. Hogan *et al.*, 2011).

Inner shelf – HH12-04

U1 was sampled by HH12-04 which locally indicates the presence of diamicton (Fig. 9). The deglacial–postglacial sediment stratigraphy of the inner shelf is, however, poorly developed, with < 3 m of U4 locally draped over U1 (Fig. 9). U4 was sampled by HH12-04, which indicates finer grain size of the mud matrix compared to in inner Rijpfjorden, but with a downcore increase in IRD (Fig. 4). This indicates less influence of meltwater but greater presence of drifting ice on the inner shelf compared to inner Rijpfjorden (cf. Plassen *et al.*, 2004; Hogan *et al.*, 2010b).
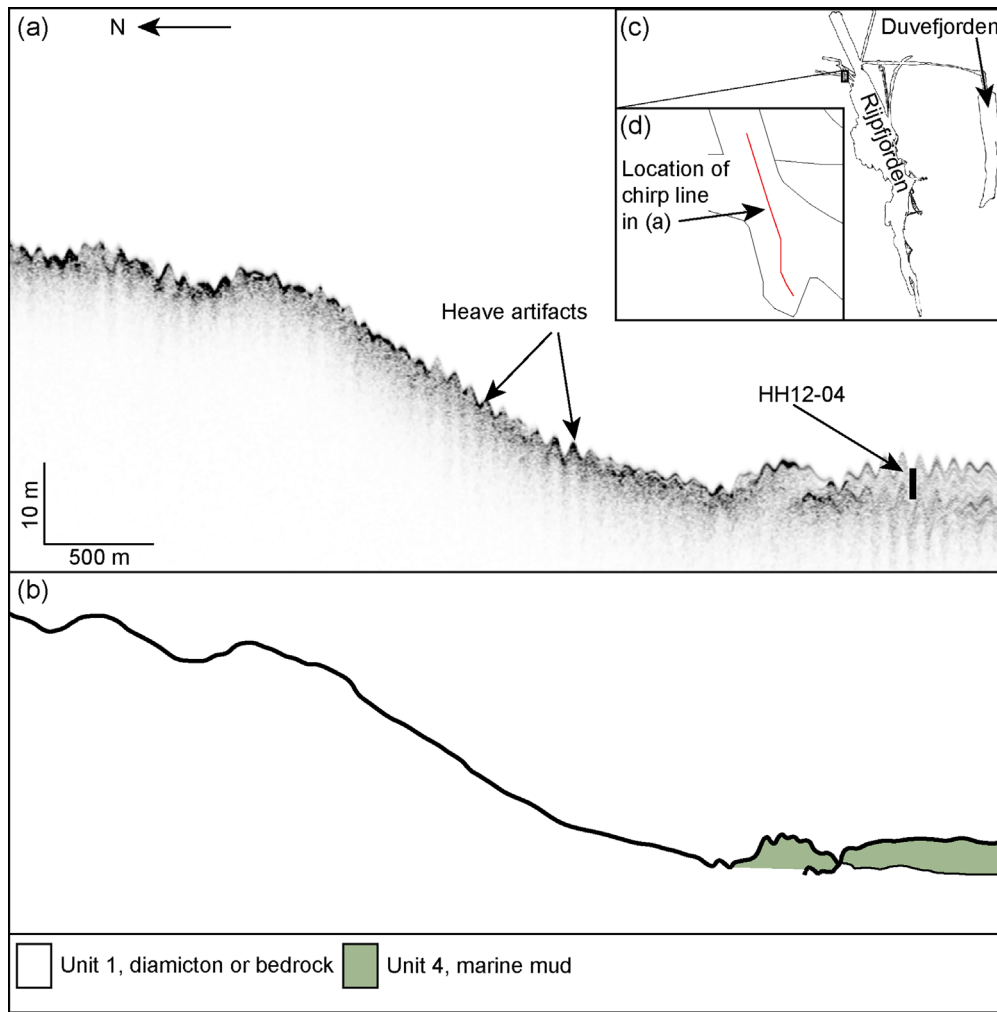
Figure 9. (a) Chirp profile showing the location and approximate penetration depth of core HH12-04 (arrowed). (b) Interpretation of the chirp profile in (a) based on the acoustic facies analysis of the chirp data and the lithology of HH12-04. (c,d) The location of the chirp profile, which is marked with a red line in (d).

Central Duvefjorden – HH11-12

Central Duvefjorden is dominated by a sediment accumulation basin for deglacial–postglacial sediments reaching 26 m in thickness (Figs 6 and 10). The base of HH11-12 sampled U3, indicating a distal glacimarine environment with the presence of drifting ice (Fig. 5). The fine grain size and the ^{14}C ages of U4 indicate Holocene deposition through suspension settling (cf. Hogan et al., 2011). Mass-flow deposits are present in and on top of the glacimarine laminated mud as well as within the marine mud, indicating mass-flows during the deglaciation (Fig. 10). The mass-flow deposit interpretations are supported by their location next to steep slopes in the bathymetry (Fig. 10) (Hogan et al., 2011). Gas in sediment often gives similar acoustic characteristics to mass-flow deposits, but gas is considered unlikely because more chimney-like geometries could be expected (e.g. Roy et al., 2014).

Bathymetric data

Longitudinal landforms

Description

Crudely streamlined longitudinal landforms are common on submarine elevations in Rijpfjorden, Duvefjorden and on the adjacent inner continental shelf (Figs 11 and 12). These landforms are characteristic to the areas with scarce sediment cover (Figs 6, 11 and 12). In the inner Rijpfjorden, the crudely streamlined landforms have a S–N orientation that gradually changes to SSW–NNE in its central and outer parts (Fig. 11).

At water depths of 100–210 m on the inner shelf off Rijpfjorden, the crudely streamlined longitudinal landforms transform into a series of parallel landforms with blunt and wide southern parts and narrowing northern parts (Fig. 12a). These landforms have a SSW–NNE orientation and reach dimensions of 1100 × 160 × 30 m (length/width/height). Maximum elongation ratio of the individual landforms on the shelf is 7: 1 (Fig. 12c). The distance between the landforms of the same cluster varies from 30 to 200 m.

The crudely streamlined landforms in Duvefjorden are found in depths from 250 to 375 m and are characterized by their blunt southern and narrower northern parts (Fig. 12b). The lengths and widths of these landforms vary (from 2400 to 4400 m and 100–400 m, respectively). Their heights are between 30 and 50 m (Fig. 12b). The elongation ratios vary from 9: 1 to 20: 1. The long axis orientation varies from S–N in the inner to central fjord to SW–NE in the outer fjord. The spacing between the landforms in Duvefjorden varies from 150 to 800 m. One of the most prominent individual landforms in Duvefjorden is shown in Fig. 12d.

Streamlined fjord-parallel landforms are also observed on the inner shelf north of both Rijpfjorden and Duvefjorden. These landforms are ca. 100–200 m wide and 10 m high. Their lengths are > 1 km but reach beyond the limits of the dataset (Fig. 1b).

Interpretation

The crudely streamlined landforms in inner and outer Rijpfjorden are interpreted as bedrock-lineations that have been polished by streaming glacier-ice (Fig. 11)
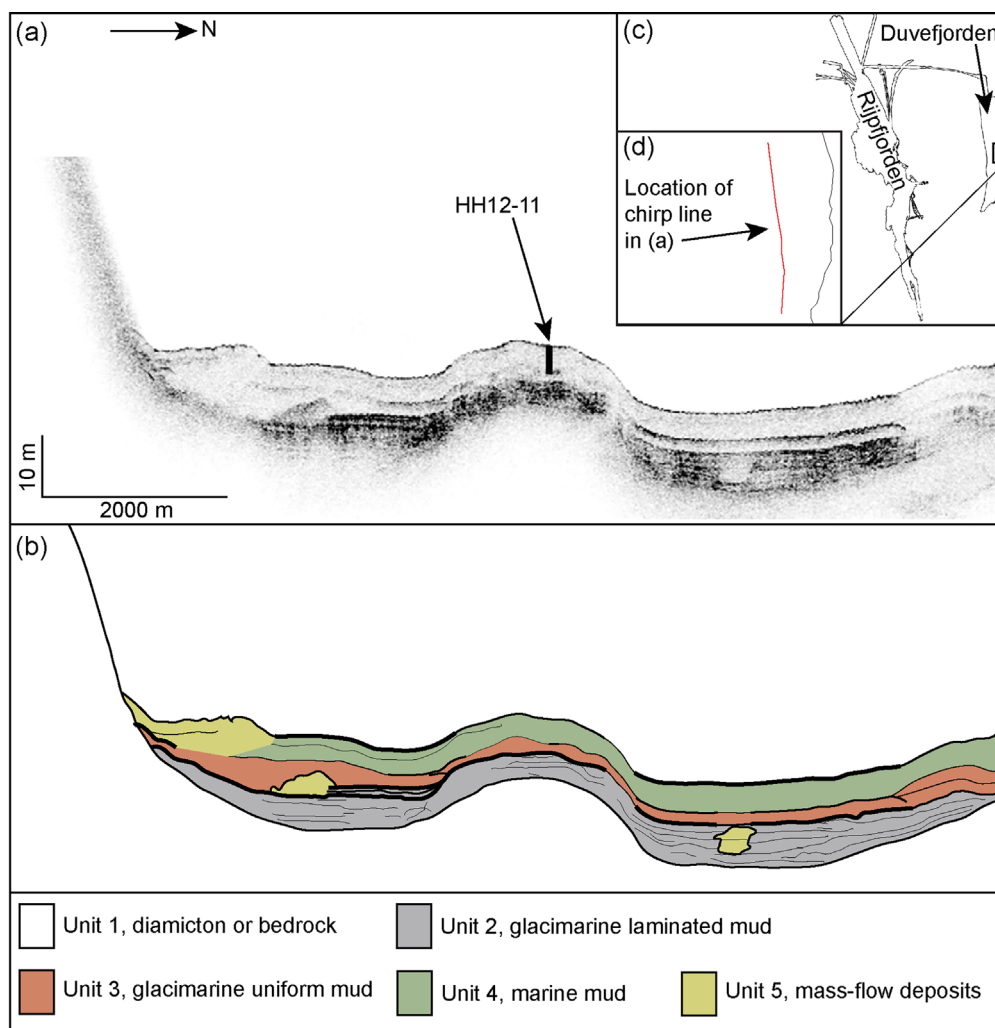
Figure 10. (a) Chirp profile showing the location and approximate penetration depth of core HH12-11 (arrowed). (b) Interpretation of the same chirp profile based on the acoustic facies analysis and the lithology of HH12-11. (c,d) The location of the chirp profile, which is marked with a red line in (d).

(Stroeven and Swift, 2008). Sub-cropping bedrock is supported by the scarce sediment cover in the chirp data (Fig. 6). The longitudinal landforms with blunt proximal and narrowing distal parts in Duvefjorden and on the inner shelf north of Rijpfjorden are interpreted as crag-and-tails, which is based on their characteristic shape and dimensions (e.g. Benn and Evans, 2010). The location of these landforms on elevated seafloor areas with sub-cropping bedrock (Fig. 6) is typical for crag-and-tails (Ottesen *et al.*, 2005; Smith *et al.*, 2006). The crag-and-tails formed at the base of streaming ice, where the long axis orientation is in the direction of palaeo-ice flow (Hogan *et al.*, 2010b). The streamlined landforms north of both Rijpfjorden and Duvefjorden are interpreted as glacial lineations that also formed at the base of streaming ice (Fig. 1b) (e.g. Stokes and Clark, 2002). The location of the glacial lineations implies that ice-flow from both Rijpfjorden and Duvefjorden continued out on the shelf (Fig. 1b).

Transverse ridges

Description

Sets of parallel ridges, roughly perpendicular to the fjord axis, occur in water depths < 210 m in Rijpfjorden and on the adjacent shelf (Figs 11b,c and 13). The ridges have maximum length/width/height of $750 \times 100 \times 5$ m, and the distance between the ridges varies from 40 to 200 m (Fig. 13). The ridges generally display symmetrical cross-profiles with slope angles of 4–12° (Fig. 11c). The ridges in

inner Rijpfjorden are covered by marine mud (Fig. 8), whereas the ridges in the central to outer Rijpfjorden are superimposed on streamlined bedrock and have a thinner sediment cover (Fig. 11c). In the deeper parts of Rijpfjorden as well as throughout the mapped area of Duvefjorden, transverse ridges are absent.

Interpretation

The transverse ridges are interpreted as De Geer moraines formed during relatively short-term still-stands or readvances of the glacier margin during the deglaciation. This is supported by the local superimposition on streamlined bedrock (Fig. 11c). The local drape of marine mud supports that the ridges formed by glacial marginal processes and later were covered by sediments deposited in a marine environment (Fig. 8). The dimensions and distances between the individual ridges are similar to the De Geer moraines described earlier from other areas by, for example, Lindén and Möller (2005) and Flink *et al.* (2015).

Grooves

Description

Grooves with V-shaped cross-sections were identified at 50–100 m water depth on the inner shelf north of Rijpfjorden (Fig. 14). These grooves have varying orientations, dimensions and cross-cutting relationships. Common widths of the grooves are 70–100 m. Their depth is usually 2–3 m (Fig. 14).
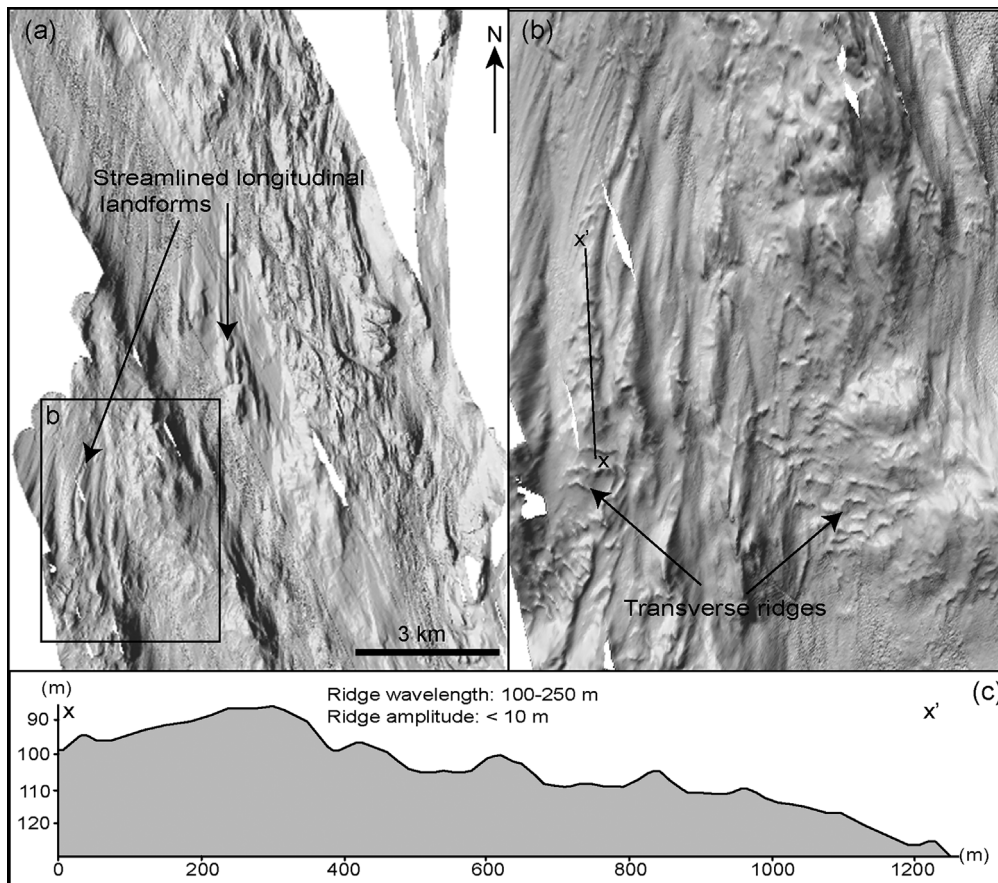
Figure 11. Central and outer Rijpfjorden are dominated by sets of streamlined longitudinal landforms (arrowed in a). (b) Prominent streamlined features are locally superimposed by parallel transverse ridges. (c) Along-profile of these transverse ridges shows their relatively symmetrical profile. Location of the area is shown in Fig. 1b.

Interpretation

The grooves on the inner shelf are commonly found on high-latitude continental margins and are interpreted as iceberg ploughmarks. Iceberg ploughmarks are formed because of seafloor scouring by floating icebergs, which originate from calving glacier fronts (e.g. Dowdeswell *et al.*, 1992).

Discussion

Ice-sheet dynamics

The submarine landform record shows that both Rijpfjorden and Duvefjorden accommodated ice streams that flowed in northerly to north-easterly directions out onto the shelf (Fig. 15). The locally deeper bathymetry northwards from the fjords (Fig. 1b) as well as the landform record in Albertini Trough and the dated sediment record at its trough mouth confirm that ice-flow continued there before it reached the continental shelf edge north of Nordaustlandet (Noormets *et al.*, 2012; Chauhan *et al.*, 2016a,b) (Fig. 1). The deeper basin and higher elongation ratios of streamlined subglacial landforms in Duvefjorden suggest that a larger and/or more focused ice-stream flowed there compared to in Rijpfjorden (Fig. 15). The comparatively well-developed trough extending out onto the inner shelf from Duvefjorden (Fig. 1b) suggests that the ice-flow from Duvefjorden reached further out onto the shelf than the ice-flow from Rijpfjorden (cf. Wellner *et al.*, 2001).

The varied depth of the Rijpfjorden basin shows relatively good correlation to the variation in costal geology (Fig. 1b). The deeper inner and central fjord basins probably consist of the surrounding sedimentary bedrock types (Fig. 1b). The relatively low resistance to glacial erosion of such bedrock probably made it possible for ice-flow to focus there,

consequently forming the deeper basins (Fig. 1b). The crudely streamlined bedrock in the central to outer Rijpfjorden and crag-and-tails on the inner continental shelf show proximity to crystalline bedrock, which is more resistant to erosion (cf. Wellner *et al.*, 2001). These areas are suggested to have been important for obstructing and slowing down the ice-flow in Rijpfjorden and on the inner continental shelf and preventing trough development (Fig. 1b).

The deeper and narrower basin of Duvefjorden probably consists of similar sedimentary bedrock as found on the adjacent Prins Oscars Land (Fig. 1b). The relatively easily erodible sedimentary bedrock facilitated the focusing of the ice-flow in the narrower trough, potentially resulting in a build-up of a larger and faster ice stream due to easier passage compared to Rijpfjorden (cf. Wellner *et al.*, 2001). In addition, the E–W-trending faults on the eastern part of Prins Oscars Land probably extend into the basin of Duvefjorden, which is suggested to have facilitated ice-flow there (Fig. 1b). Based on the IBCAO (Jakobsson *et al.*, 2012), it is likely that the ice stream in Duvefjorden flowed out onto the continental shelf and eroded a distinct trough there that continues over 30 km north of the fjord (Figs 1b and 15). This supports our interpretation that Duvefjorden accommodated a somewhat larger ice stream than Rijpfjorden, although both were probably significant outlets draining the SBIS (Fig. 1b).

Deglaciation

The presence of De Geer moraines in areas shallower than 210 m on the inner continental shelf and in Rijpfjorden indicate a relatively slow and punctuated retreat of the ice margin there (Fig. 15). The timing of the formation of the De Geer moraines is uncertain. However, if assuming annual formation, the retreat of the ice margin is estimated to
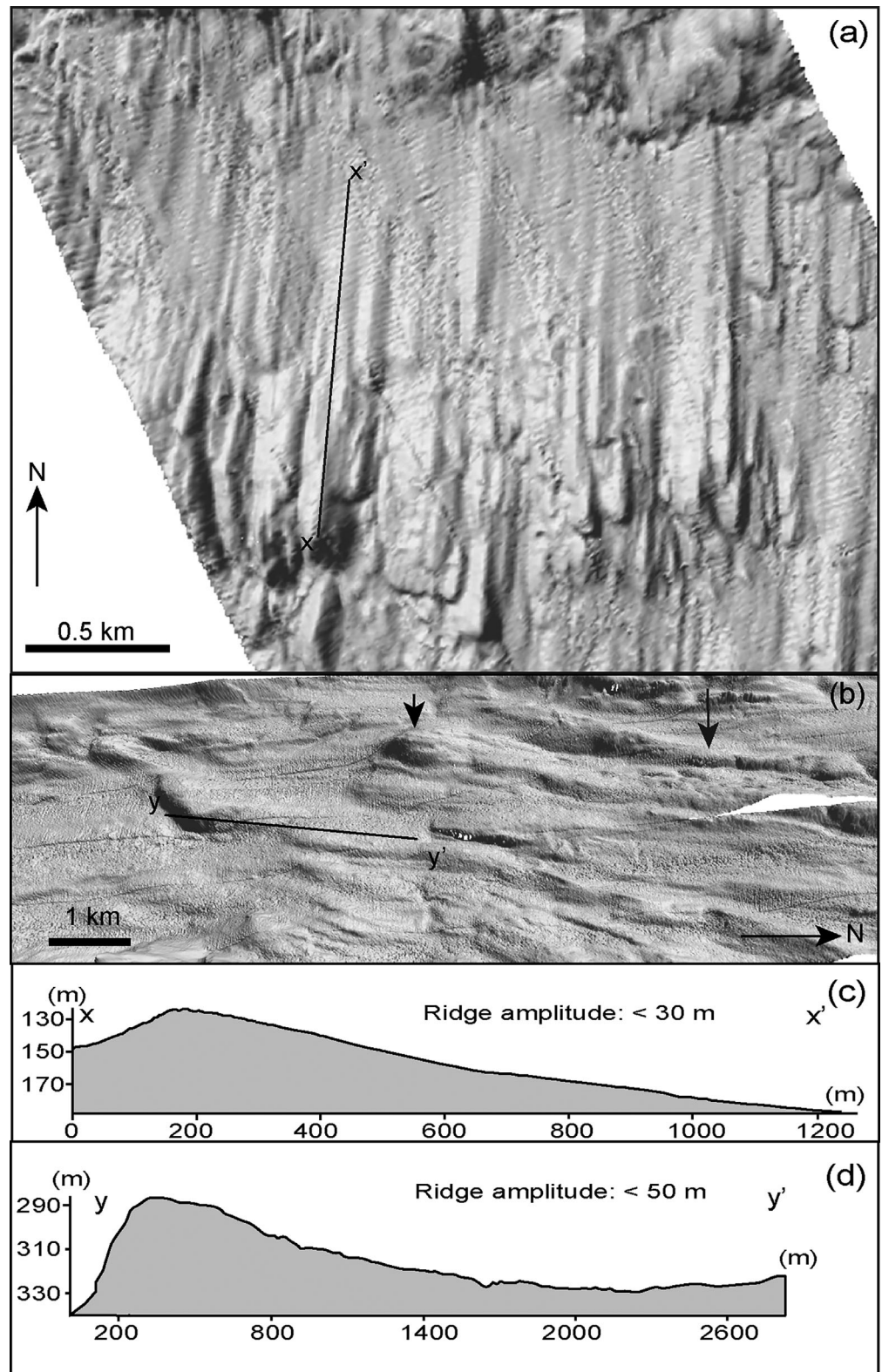
Figure 12. (a)The inner shelf off Rijpfjorden is dominated by parallel elongated landforms with blunt proximal and narrower distal parts with SSW–NNE orientation. (b) Duvefjorden is dominated by elongated landforms (arrowed) with blunt proximal and narrower distal sides. Their elongation ratios vary from 9: 1 to 20: 1. (c) Along-profile of one of the most prominent elongated landforms on the inner shelf off Rijpfjorden. (d) Along-profile of one of the most prominent elongated landforms found in the central Duvefjorden. Locations of the areas are shown in Fig. 1b.

100–250 m a^{-1} in the areas where De Geer moraines are present (Fig. 15). Annual formation of De Geer moraines has earlier been suggested based on relatively even spacing between moraines in Borebukta and Tempelfjorden (Ottesen and Dowdeswell, 2006; Flink et al., 2015). Deeper areas of Rijpfjorden and Duvefjorden lack retreat-related landforms in both the bathymetric and the chirp data, which suggest that those areas featured floating ice margins during the deglaciation (Fig. 15). The iceberg ploughmarks on the inner shelf north of Rijpfjorden and Duvefjorden suggest that the floating margins disintegrated mainly through calving (Fig. 15). In

particular, the deep fjord basin of Duvefjorden was probably of importance for iceberg production and transportation out to the continental shelf north of Nordaustlandet (Fig. 1b) where a high abundance of iceberg ploughmarks has been reported (Noormets et al., 2012). Also at modern times, calving has been suggested as the dominating mechanism of retreat of the Austfonna ice cap margin (Moholdt et al., 2010).

Samples obtained from glacimarine mud in the inner Rijpfjorden and central Duvefjorden yielded the oldest ^{14}C ages (Table 1). These ages indicate that the innermost part of Rijpfjorden and the central Duvefjorden were
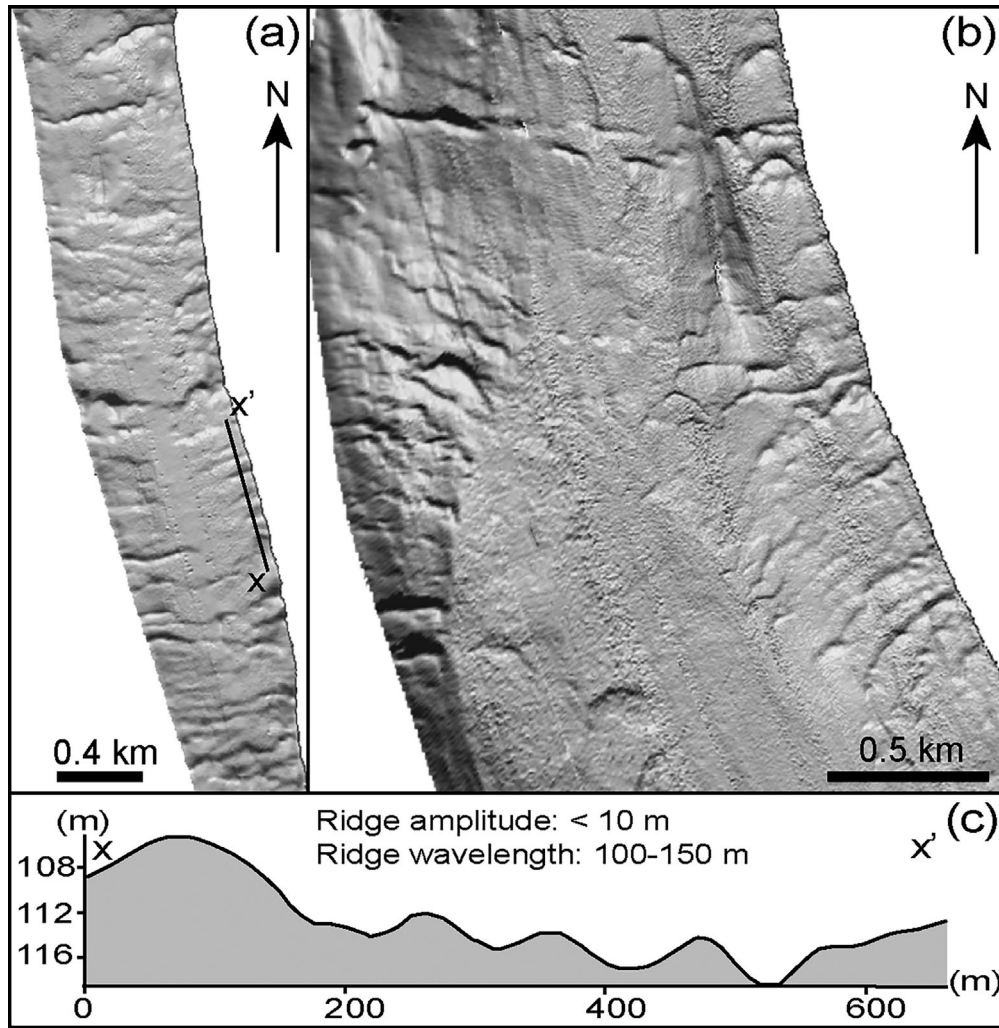
Figure 13. (a,b) The inner Rijpfjorden is dominated by semi-parallel, transverse ridges with maximum length/width/height of $750 \times 100 \times 10$ m. The ridges occur in water depths of <210 m. (c) Distance between the transverse ridges is between 100 and 150 m. For location, see Fig. 1b.

deglaciated ca. 10.6 and 11.0 cal a BP, respectively (Table 1). The somewhat earlier deglaciation of Duvefjorden could be attributed to its deeper central basin facilitating faster retreat of the ice margin through calving (Fig. 1b).

The basal meltout-till with embedded plume deposits at the base of core HH12-04 indicate basal melting during retreat over the inner shelf (cf. Powell, 1984). The gradual decrease of IRD from the base to top in HH12-04 suggests a decreased
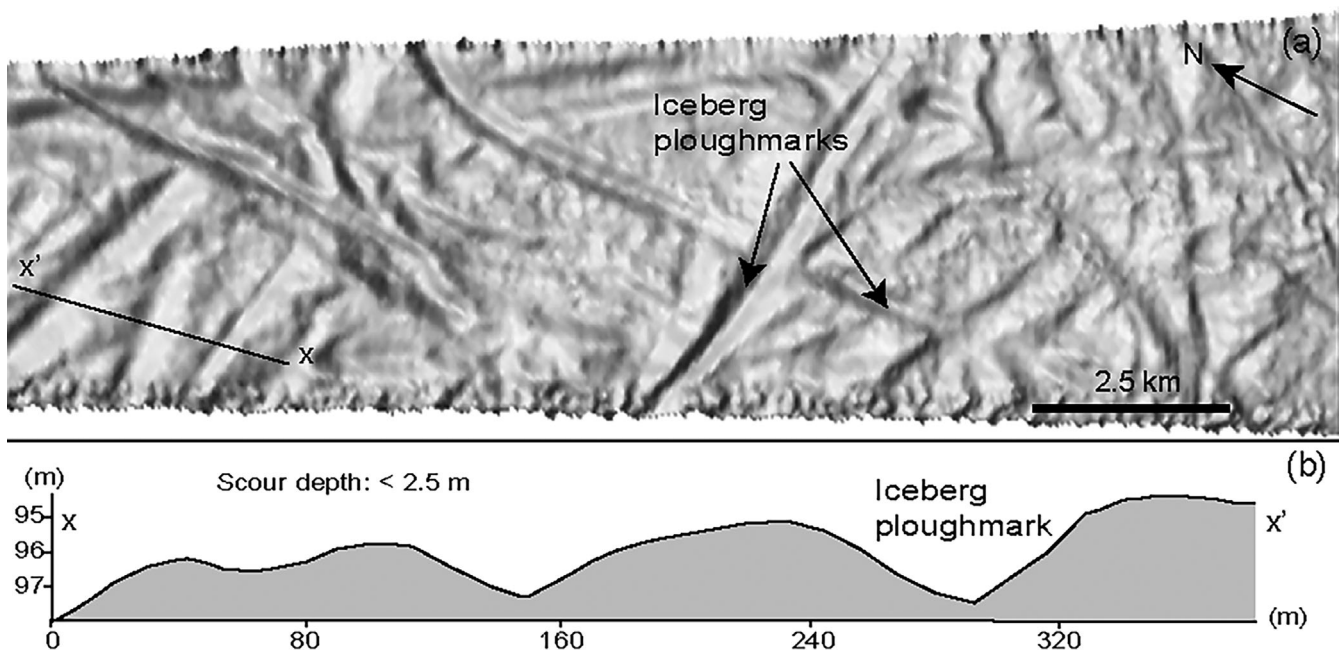

Figure 14. (a) Grooves are found on the inner shelf north of Rijpfjorden. (b) V-shaped cross-sections of the grooves are up to 2.5 m deep. For location of the area, see Fig. 1b.
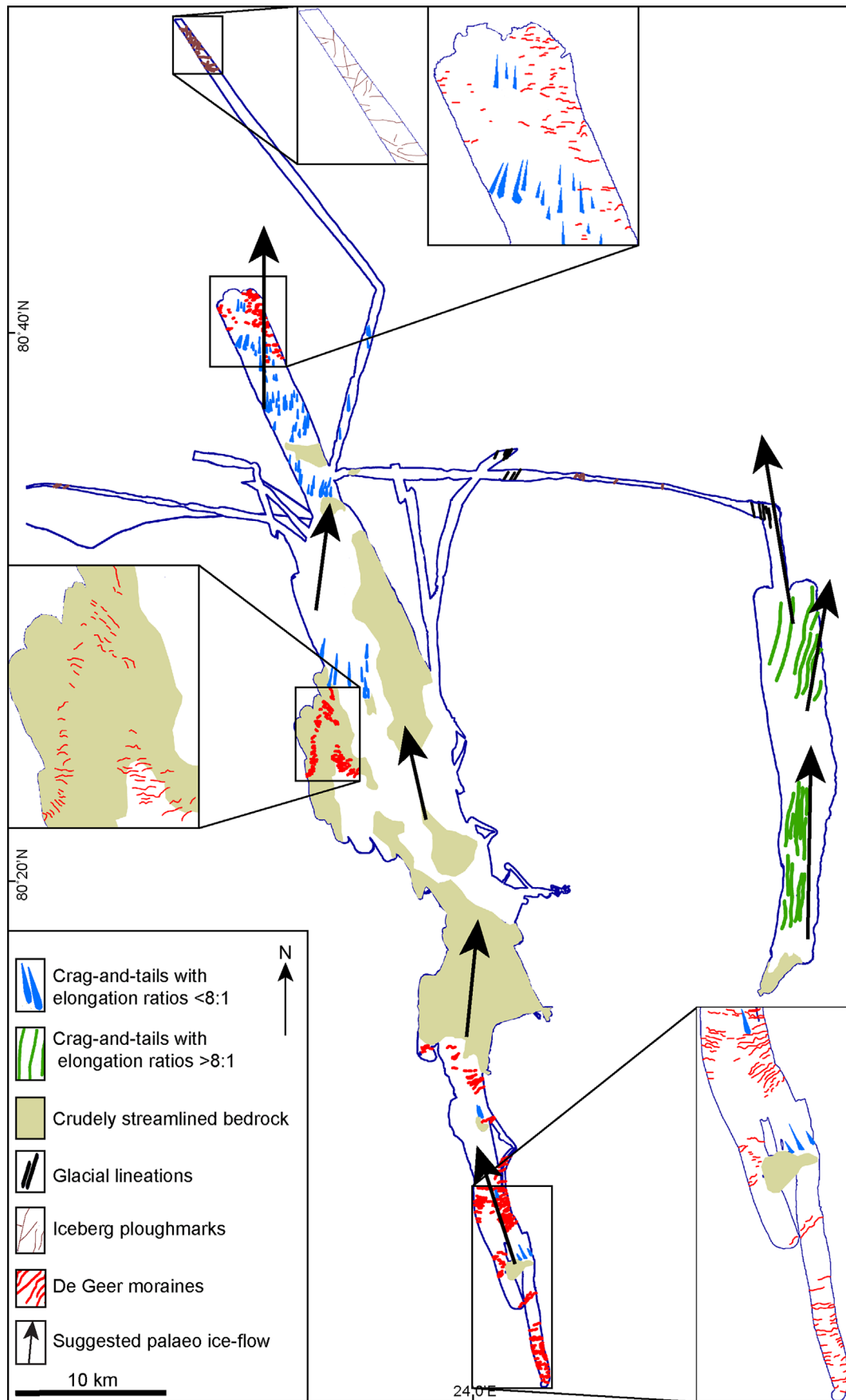
Figure 15. Distribution of major glacial landforms in Rijpfjorden and Duvefjorden. Palaeo ice-flow directions are indicated with arrows.

calving rate of the glacier front and a gradual transition from glacimarine to a marine environment (cf. Elverhøi and Solheim, 1983). The thickest postglacial sediment sequences correspond to deeper bathymetry in Rijpfjorden and Duvefjorden (Fig. 6). This shows that the areas of greatest glacial erosion became sediment accumulation basins after the deglaciation (Fig. 6). Mass-flow deposits are mainly recorded in the deep basin of Duvefjorden (Fig. 6), indicating that the steep basin walls facilitated gravity-driven mass-flows (cf. Syvitski et al., 1987). The upward decrease in sedimentation rates in core HH11-02 suggests a gradually increasing distance to the glacier front into a marine environment during the Holocene (Table 1). However, the four mass-flow deposits in the core indicate mass-flow events throughout the Holocene probably influenced by increased meltwater input, which is supported by the relatively coarse matrix surrounding the mass-flow deposits (Fig. 2). Increased meltwater input could be explained by the proximity of the coring site to the coastline, resulting in direct input from glacially fed rivers (Fig. 1b). However, the relatively low variations in magnetic susceptibility in HH11-02 may indicate a relatively stable drainage area of the glacially fed rivers that reached Rijpfjorden (Fig. 2).

The decreased sedimentation rate from the deglaciation until the mid-Holocene and the general fining of sediments upwards in core HH12-11 suggest a gradual change from a higher-energy glacimarine to lower-energy marine environment (Table 1). The following increase in sedimentation rate correlates with increased magnetic susceptibility values for the top 170 cm of core HH12-11 (Fig. 5; Table 1), which suggests increased melt-off, changed lithology and potentially changed sediment source (Robinson et al., 1995; Plassen et al., 2004). This could indicate somewhat more dynamic drainage patterns for Austfonna compared to Vestfonna if they were separated during the mid- to late Holocene.

Conclusions

Based on analysis of the distribution and geometry of submarine landforms and the lithology and stratigraphy of the sediments, the ice sheet dynamics and deglacial history of Rijpfjorden, Duvefjorden and their adjacent shelf have been reconstructed.

- Submarine landform patterns suggest streaming ice which was topographically controlled in Rijpfjorden and Duvefjorden. Ice-flow was S–N in the inner Rijpfjorden changing to SSW–NNE in the outer fjord. In Duvefjorden ice-flow was S–N in the inner fjord, spreading laterally from S–N to SW–NE in the outer fjord.
- Duvefjorden probably accommodated a somewhat larger ice stream and/or more focused ice-flow compared to that in Rijpfjorden. This has been attributed to the bedrock geology and its structures.
- The deglaciation of Rijpfjorden and Duvefjorden was relatively slow and punctuated in areas shallower than ca. 210 m. The retreat rate of the ice margin there is estimated to 100–250 m a^{-1} based on the spacing between the De Geer moraines. Floating ice margin conditions probably existed in deeper parts of the fjords where the ice margin disintegrated through calving. The calving process produced large icebergs that generated the numerous ploughmarks across the shelf.
- The deglaciation of the inner Rijpfjorden was complete by ca. 10.6 cal a BP, whereas the central Duvefjorden was glacier ice-free by ca. 11.0 cal a BP. The timing of the deglaciation of the northern Svalbard shelf is therefore estimated to ca. 8 ka.
- The areas of Rijpfjorden and Duvefjorden that were most heavily eroded by streaming ice became sediment accumulation basins after the deglaciation. Sediment massflows were promoted there during the Holocene due to the steep slopes of the eroded basins.

Abbreviations. IRD, ice-rafted debris; LGM, Last Glacial Maximum; SBIS, Svalbard–Barents Sea Ice Sheet; SSAMS, single stage accelerator mass spectrometry; TWT, two-way travel time.

References

Alley RB, Blankenship DD, Bentley CR et al. 1987. Till beneath ice stream B: 3. Till deformation: evidence and implications. *Journal of Geophysical Research* **92**: 8921–8929.

Andreassen K, Laberg JS, Vorren TO. 2008. Seafloor geomorphology of the SW Barents Sea and its glaci-dynamic implications. *Geomorphology* **97**: 157–177.

Andreassen K, Nilssen LC, Rafaelsen B et al. 2004. Three-dimensional seismic data from the Barents Sea margin reveal evidence of past ice streams and their dynamics. *Geology* **32**: 729–732.

Batchelor CL, Dowdeswell JA. 2014. The physiography of high Arctic cross-shelf troughs. *Quaternary Science Reviews* **92**: 68–96.

Batchelor CL, Dowdeswell JA, Hogan KA. 2011. Late Quaternary ice flow and sediment delivery through Hinlopen Trough, Northern Svalbard margin: submarine landforms and depositional fan. *Marine Geology* **284**: 13–27.

Benn DI, Evans DJA. 2010. *Glaciers and Glaciation, 2nd edn.* Routledge: New York.

Bjarnadóttir LR, Rüther DC, Winsborrow MCM et al. 2013. Grounding-line dynamics during the last deglaciation of Kveithola, W Barents Sea, as revealed by seabed geomorphology and shallow seismic stratigraphy. *Boreas* **42**: 84–107.

Bond GC, Lotti R. 1995. Iceberg discharges into the North Atlantic on millennial time scales during the last glaciation. *Science* **267**: 1005–1010.

Chauhan T, Noormets R, Rasmussen TL. 2016b. Glaciomarine sedimentation and bottom current activity on the north-western and northern continental margins of Svalbard during the late Quaternary. *Geo-Marine Letters* **36**: 81–99.

Chauhan T, Rasmussen TL, Noormets R et al. 2014. Glacial history and paleoceanography of the southern Yermak Plateau since 132 ka BP. *Quaternary Science Reviews* **92**: 155–169.

Chauhan T, Rasmussen TL, Noormets R. 2016a. Palaeoceanography of the Barents Sea continental margin, north of Nordaustlandet, Svalbard, during the last 74 ka. *Boreas* **45**: 76–99.

Dallmann WK, Ohta Y, Elvevold S et al., eds. 2002. Bedrock map of Svalbard and Jan Mayen. *Norsk Polarinstitutt Temakart* No. 33.

Dowdeswell JA, Jakobsson M, Hogan KA et al. 2010. High-resolution geophysical observations of the Yermak Plateau and northern Svalbard margin: implications for ice-sheet grounding and deep-keeled icebergs. *Quaternary Science Reviews* **29**: 3518–3531.

Dowdeswell JA, Whittington RJ, Hodgkins R. 1992. The sizes, frequencies, and freeboards of East Greenland icebergs observed using ship radar and sextant. *Journal of Geophysical Research* **97**: 3515–3528.

Dreimanis A. 1979. The problems of waterlain tills. In *Moraines and Varves*, Schlüchter, C (eds). Balkema: Rotterdam; 167–177.

Elverhøi A, Lauritzen O. 1984. Bedrock geology of the northern Barents Sea (west of 35° E) as inferred from the overlying Quaternary deposits. *Norsk Polarinstitutt Skrifter* **180**: 5–16.

Elverhøi A, Pfirman SL, Solheim A et al. 1989. Glaciomarine sedimentation in epicontinental seas exemplified by the northern Barents Sea. *Marine Geology* **85**: 225–250.

Elverhøi A, Solheim A. 1983. The Barents Sea ice sheet – a sedimentological discussion. *Polar Research* **1**: 23–42.

Faleide JI, Solheim A, Fiedler A *et al.* 1996. Late Cenozoic evolution of the western Barents Sea-Svalbard continental margin. *Global and Planetary Change* **12**: 53–74.

Flink AE, Noormets R, Kirchner N *et al.* 2015. The evolution of a submarine landform record following recent and multiple surges of Tunabreen glacier, Svalbard. *Quaternary Science Reviews* **108**: 37–50.

Flood B, Gee DG, Hjelle A *et al.* 1969. The geology of Nordaustlandet, northern and central parts. *Norsk Polarinstitutt Skrifter* **146**.

Hagen JO, Liestøl O, Roland E *et al.* 1993. Glacier atlas of Svalbard and Jan Mayen. *Norwegian Polar Institute Meddelelser* **129**. Oslo.

Harland WB, Herod KN, Krinsley DH. 1966. The definition and identification of tills and tillites. *Earth-Science Reviews* **2**: 225–256.

Hjelstuen BO, Kjennbakken H, Bleikli V *et al.* 2013. Fjord stratigraphy and processes – evidence from the NE Atlantic Fensfjorden system. *Journal of Quaternary Science* **28**: 421–432.

Hogan KA, Dix JK, Lloyd JM *et al.* 2011. Seismic stratigraphy records the deglacial history of Jakobshavn Isbræ, West Greenland. *Journal of Quaternary Science* **26**: 757–766.

Hogan KA, Dowdeswell JA, Noormets R *et al.* 2010a. Evidence for full-glacial flow and retreat of the Late Weichselian Ice Sheet from the waters around Kong Karls Land, eastern Svalbard. *Quaternary Science Reviews* **29**: 3563–3582.

Hogan KA, Dowdeswell JA, Noormets R *et al.* 2010b. Submarine landforms and ice-sheet flow in the Kvitøya Trough, northwestern Barents Sea. *Quaternary Science Reviews* **29**: 3345–3562.

Jakobsson M, Mayer L, Coakley B *et al.* 2012. The international bathymetric chart of the Arctic Ocean (IBCAO) Version 3.0. *Geophysical Research Letters* **39**.

Johansson A, Gee DG, Larionov AN *et al.* 2005. Grenvillian and Caledonian evolution of eastern Svalbard – a tale of two orogenies. *Terra Nova* **17**: 317–325.

Knies J, Kleiber HP, Matthiessen J *et al.* 2001. Marine ice-rafted debris records constrain maximum extent of Saalian and Weichselian ice-sheets along the northern Eurasian margin. *Global and Planetary Change* **31**: 45–64.

Knies J, Vogt C, Stein R. 1998. Late Quaternary growth and decay of the Svalbard/Barents Sea ice sheet and paleoceanographic evolution in the adjacent Arctic Ocean. *Geo-Marine Letters* **18**: 195–202.

Koc N, Klitgaard-Kristensen D, Hasle K *et al.* 2002. Late glacial palaeoceanography of Hinlopen Strait, northern Svalbard. *Polar Research* **21**: 307–314.

Landvik JY, Ingólfsson Ó, Mienert J *et al.* 2005. Rethinking Late Weichselian ice-sheet dynamics in coastal NW Svalbard. *Boreas* **34**: 7–24.

Lindén M, Möller P. 2005. Marginal formation of De Geer moraines and their implications to the dynamics of grounding-line recession. *Journal of Quaternary Science* **20**: 113–133.

Löwemark L, Schönfeld J, Schäfer P. 2006. Deformation of pyritized burrows: a novel technique for the detection and estimation of core shortening in gravity cores. *Marine Geology* **233**: 37–48.

Mangerud J, Dokken T, Hebbeln D *et al.* 1998. Fluctuations of the Svalbard-Barents Sea ice sheet during the last 150000 years. *Quaternary Science Reviews* **17**: 11–42.

Moholdt G, Hagen JO, Eiken T *et al.* 2010. Geometric changes and mass balance of the Austfonna ice cap, Svalbard. *The Cryosphere* **4**: 21–34.

NAD Science Committee. 1992. The Arctic Ocean record: key to global change – initial science plan of the Nansen Arctic Drilling Program. *Polarforschung* **161**.

Noormets R, Hogan K, Austin W *et al.* 2012. Submarine glacial landform assemblages on the outer continental shelf north of Nordaustlandet, Svalbard. In *The 6th Arctic Paleoclimate and its Extremes (APEX) Meeting, Program and Abstracts*, Oulu University, 15–18 May. Oululanka Research Station, Finland; 70.

Ottesen D, Dowdeswell JA. 2006. Assemblages of submarine landforms produced by tidewater glaciers in Svalbard. *Journal of Geophysical Research* **111**: F1.

Ottesen D, Dowdeswell JA, Landvik JY *et al.* 2007. Dynamics of the Late Weichselian ice sheet on Svalbard inferred from high-resolution seafloor morphology. *Boreas* **36**: 287–306.

Ottesen D, Dowdeswell JA, Rise L. 2005. Submarine landforms and the reconstruction of fast-flowing ice streams within a large Quaternary ice sheet: the 2500-km-long Norwegian-Svalbard margin (57°–80°N). *Geological Society of America Bulletin* **117**: 1033–1050.

Patton H, Andreassen K, Bjarnadóttir LR *et al.* 2015. Geophysical constraints on the dynamics and retreat of the Barents Sea ice sheet as a paleobenchmark for models of marine ice sheet deglaciation. *Reviews of Geophysics* **53**: 1051–1098.

Plassen L, Vorren TO, Forwick M. 2004. Integrated acoustic and coring investigation of glacigenic deposits in Spitsbergen fjords. *Polar Research* **23**: 89–110.

Powell RD. 1984. Glacimarine processes and inductive lithofacies modelling of ice shelf and tidewater glacier sediments based on Quaternary examples. *Marine Geology* **57**: 1–52.

Rebesco M, Laberg JS, Pedrosa MT *et al.* 2014. Onset and growth of trough-mouth fans on the north-western Barents Sea margin– implications for the evolution of the Barents Sea/Svalbard Ice Sheet. *Quaternary Science Reviews* **92**: 227–234.

Reimer PJ, Bard E, Bayliss A *et al.* 2013. IntCal13 and Marine13 radiocarbon age calibration curves 0–50, 000 years cal BP. *Radiocarbon* **55**: 1869–1887.

Rignot E, Kanagaratnam P. 2006. Changes in the velocity structure of the Greenland ice sheet. *Science* **311**: 986–990.

Robinson P, Dowdeswell JA. 2011. Submarine landforms and the behavior of a surging ice cap since the last glacial maximum: the open-marine setting of eastern Austfonna, Svalbard. *Marine Geology* **286**: 82–94.

Robinson SG, Maslin MA, McCave IN. 1995. Magnetic susceptibility variations in Upper Pleistocene deep-sea sediments of the NE Atlantic: implications for ice rafting and paleocirculation at the last glacial maximum. *Paleoceanography* **10**: 221–250.

Roy S, Senger K, Braathen A *et al.* 2014. Fluid migration pathways to seafloor seepage in inner Isfjorden and Adventfjorden, Svalbard. *Norwegian Journal of Geology*: 99–119.

Rüther DC, Mattingsdal R, Andreassen K *et al.* 2011. Seismic architecture and sedimentology of a major grounding zone system deposited by the Bjørnøyrenna Ice Stream during Late Weichselian deglaciation. *Quaternary Science Reviews* **19**: 2776–2792.

Siegert MJ, Dowdeswell JA, Hald M *et al.* 2001. Modelling the Eurasian Ice Sheet through a full (Weichselian) glacial cycle. *Global and Planetary Change* **31**: 367–385.

Smith MJ, Rose J, Booth S. 2006. Geomorphological mapping of glacial landforms from remotely sensed data: an evaluation of the principal data sources and an assessment of their quality. *Geomorphology* **76**: 148–165.

Stokes CR, Clark CD. 2002. Are long subglacial bedforms indicative of fast ice flow? *Boreas* **31**: 239–249.

Stokes CR, Tarasov L, Blomdin RL *et al.* 2015. On the reconstruction of palaeo-ice sheets: recent advances and future challenges. *Quaternary Science Reviews* **125**: 15–49.

Stroeven AP, Swift DA. 2008. Glacial landscape evolution – implications for glacial processes, patterns and reconstructions. *Geomorphology* **97**: 1–4.

Syvitski JPM, Burrell DC, Skei JM. 1987. *Fjords – Processes and Products*. Springer Verlag: New York.

Wellner JS, Lowe AL, Shipp SS *et al.* 2001. Distribution of glacial geomorphic features on the Antarctic continental shelf and correlation with substrate: implications for ice behavior. *Journal of Glaciology* **47**: 397–411.

Winsborrow MCM, Andreassen K, Corner GD *et al.* 2010. Deglaciation of a marine-based ice sheet: Late Weichselian palaeo-ice dynamics and retreat in the southern Barents Sea reconstructed from onshore and offshore glacial geomorphology. *Quaternary Science Reviews* **29**: 424–442.